Effects of the Distribution of Synaptic Strength of Neuronal Network on its Spiking Dynamics

Yeung Chun Yat (1155110319)

Supervisor: Prof. Ching Shuk Chi Emily

December, 2020

Abstract

Networks are prevalent in sciences. This research project studies neuronal networks in particular, which have spiking dynamics that is highly skewed and long-tailed in distribution, showing a significant deviation from Gaussian. In our model, the network dynamics associates with the network structure through a system of dynamical equations that governs the evolution of the nodal states. In the neuronal network studied, the synaptic strengths, like the spike counts, also have a skewed and long-tailed distribution, and whether the two are associated, either statistically or causally, is the central question to answer. In this project, different useful measures of a network are first explained, and a network reconstruction method using only the neuronal time series data is reviewed and presented. Based on the reconstructed network structure, different combinations of dynamical functions are attempted, and the behavior of each network model is studied. It is found that the FitzHugh-Nagumo network model combined with the synaptic nodal interaction has the best performance, succeeding in generating realistic neuronal spikes which recover some empirical statistical features that real neuronal spikes have. Finally, the effects of the distribution of synaptic strength on the spiking dynamics are investigated, and the analysis indicates that the long-tailed incoming strengths are causing the long-tailed spike counts.

Contents

1 Project Overview

The project consists of the following four parts.

(1) (*Literature Review*) A network reconstruction method, proposed by Ching and Tam, that uses empirical time series data to establish the (underlying) links and coupling strengths between nodes is reviewed. The method bases itself on a noise-induced relation from which the network connectivity can be retrieved.

(2) (*An Example Study*) The network reconstruction method reviewed is applied to a small directed weighted random network of 100 nodes. The nature of the network dynamics, along with its dynamical functions and the algorithm for generating the time series, is discussed, and the result proposed by the method is verified.

(3) (*Model Testing*) Two models, each obeying a different intrinsic dynamics, are tested. One obeys *logistic* and the other obeys *FitzHugh-Nagumo*. The natures of the model time series generated are examined, and we shall see that the former *fails* at generating realistic neuronal spikes while the latter *succeeds* in giving realistic results while recovering *some* of the empirical statistical features.

(4) (*Analysis*) It is observed that the experimental neuronal spike counts are highly skewed and long-tailed in distribution, and so are the synaptic strengths. Researchers have long conjectured that there exists some association between the two, and that the distribution of the synaptic strengths affects the distribution of spike counts – *Can the very large spike counts be explained by the very large synaptic strengths?* It inevitably requires a model to establish the connection between the network structure and the spiking dynamics. Built upon the FitzHugh-Nagumo network model, the effects of different network features, including degrees and strengths, on the spiking dynamics are investigated, through *regression analysis* and the use of *reference networks* which preserve some features while varying some other.

Objectives. This research aims to address the following questions. They are in a broad sense, and the specific context under which they are to be understood will be supplied.

(1) For an assumed network model, how does the distribution of synaptic strengths (and more generally, the "structure" of the network) affect the spiking dynamics?

(2) A search for realistic models of neurons – How do different network models behave and perform? How do they compare in terms of resemblance to real, experimental neuronal time series?

2 Introduction

Networks [1] are prevalent in sciences, and are useful for modeling systems consisting of mutually interacting individual components. For example, connection of individuals that may be friends of each other in a social networking site and connection of websites that lead to each other on the internet may both be modeled (or abstracted) in the form of a network. Here, we study a biological example – **neuronal network**. In a network, individual components, known as **nodes**, connect to one another via **links** (or **edges**). Each node is identified with a label i, where $i = 1, 2, ..., N$ with N being the total number of nodes. Interaction between two linking nodes is quantified by the **coupling strength** that informs how strong the connection is. Often a node can affect the dynamics of another node but its own dynamics is not affected by the latter. (The meaning of "dynamics" will be made precise later.) Such behavior is captured in a **directed network** with directional links. In an **undirected network**, in contrast, the interaction between two nodes is mutual and symmetric with a two-way link. The structure of a network is a crucial piece of information for understanding the system it represents, e.g. how the individuals are interconnected, and the presence of "central bodies", known as **hubs**, that make many connections to other individuals.

In a neuronal network, each node carries a value symbolizing the electrical signal generated by the neuron at a point in time. The measured signals vary in time, sometimes with steady fluctuations and sometimes with significant jumps, which are known as **neuronal spikes** (or **peaks**). Over time, we collect the values into a time series, and the time series of all the nodes in the network collectively are called the **network dynamics**. More generally, it refers to the time-dependence or the evolution of certain network characteristics. There are many possible ways to characterize the nature of a dynamics. For a neuronal dynamics, for example, we may count the number of spikes, compute the standard deviation of the fluctuation in the time series, or measure the correlation between the time series. The characterizations are specific to the problem we want to address, and there is no characterization that is universally good. It is worth noting that each characterization has its own flaws. For example, to count spikes, we use a peak detection algorithm but it inevitably misses some spikes that are not "obvious" enough; also, standard deviation may not be a representative measure of the fluctuation in time series when the values are long-tailed in distribution.

The coupling strengths of the edges in a network are the primitive and leading factor to drive the dynamics. A node impacts its connecting nodes through the edges, with a positive coupling strength effecting an **excitatory** impact and a negative coupling strength effecting an **inhibitory** impact.

2.1 Measures of a Network

There are useful measures to aid us in understanding a network. The most important two are the **degrees** and **strengths**. The number of nodes that connect to a specific node i is known as the incoming degrees of the node i, or **in-degrees**. Likewise, the number of nodes that a specific node i connects to is known as the outgoing degrees of the node i, or **out-degrees**. Strengths are an average measure of the coupling strengths. The incoming strengths, or **in-strengths**, are the average coupling strength of edges that link to a node. The outgoing strengths, or **out-strengths**, are the average coupling strength of edges that come out of a node to other nodes.

Mathematically, we label the coupling strength of an edge that links from node j to node i by g_{ij}. As discussed, g_{ij} can be positive (meaning an excitatory edge) or negative (meaning an inhibitory edge). If node i and j are unconnected, $g_{ij} = g_{ji} = 0$, and one's dynamics does not affect the other. For a directed network, generally, $g_{ij} \neq g_{ji}$, for node j may connect to node i but not the otherwise. The coupling strengths g_{ij}, with $i, j = 1, 2, ..., N$, can be contained in an $N \times N$ **coupling strength matrix G**, which, generally, is asymmetric and sparse. In most cases, we assume the nodes are not self-connecting, so the diagonal entries of **G** are all zero. There are in total $N(N-1)$ possible directed edges in a network, and practically, most *real* networks have a number of edges that is only a tiny fraction of the number, and the fraction is known as the **sparsity**. In the neuronal network used in this project, for example, the sparsity is approximately 1.4%. *The coupling strength matrix* **G** *is the most crucial piece of information about a network*, as it specifies (1) the connectivity (i.e., where $g_{ij} \neq 0$) and (2) the nodal interactions (i.e., signs and magnitudes of g_{ij}). Other measures of the network, e.g. degrees and strengths, may be instantly derived once we have **G**. **G** has high theoretical importance, but *in practice*, it is difficult to extract and there has been ongoing research on the reconstruction of **G**, in the field of **network reconstruction**. One method to reconstruct **G** is reviewed and presented in the next section.

With **G**, we instantly know the degrees and strengths. The in-degree and out-degree of node i are respectively given by

$$k_{\text{in}}(i) = \sum_{j=1}^{N} \mathbb{1}(g_{ij} \neq 0) \text{ and } k_{\text{out}}(i) = \sum_{j=1}^{N} \mathbb{1}(g_{ji} \neq 0), \tag{1}$$

where $\mathbb{1}(\cdot)$ is the indicator function of a condition. The in-strength and out-strength of node i are respectively given by

$$s_{\text{in}}(i) = \frac{1}{k_{\text{in}}(i)} \sum_{j=1}^{N} g_{ij} \text{ and } s_{\text{out}}(i) = \frac{1}{k_{\text{out}}(i)} \sum_{j=1}^{N} g_{ji}. \tag{2}$$

Computationally, regarding the coupling strength matrix **G**, $k_{\text{in}}(i)$ is the number of non-zero entries in row i and $k_{\text{out}}(i)$ is the number of non-zero entries in column i. Similarly, $s_{\text{in}}(i)$ averages the non-zero entries in row i and $s_{\text{out}}(i)$ averages the non-zero entries in column i. There are other finer measures that could be derived. For example, if we are interested in the positive entries, we may define the positive in/out-degree and the positive in/out-strength by

$$k^{+}_{\text{in}}(i) = \sum_{j=1}^{N} \mathbb{1}(g_{ij} > 0) \text{ and } k^{+}_{\text{out}}(i) = \sum_{j=1}^{N} \mathbb{1}(g_{ji} > 0), \tag{3}$$

and

$$s^{+}_{\text{in}}(i) = \frac{1}{k^{+}_{\text{in}}(i)} \sum_{j=1}^{N} g_{ij}\mathbb{1}(g_{ij} > 0) \text{ and } s^{+}_{\text{out}}(i) = \frac{1}{k^{+}_{\text{out}}(i)} \sum_{j=1}^{N} g_{ji}\mathbb{1}(g_{ji} > 0). \tag{4}$$

This is generalizable to other desired conditions by replacing the arguments in the indicator functions. Note that for a directed network, the in- and out-measures are generally different, while for an undirected (aka. bidirectional) network, they are equivalent because of the symmetric $\mathbf{G}$.

It is also a common practice to define the adjacency matrix $\mathbf{A}$, with entry $A_{ij} = \mathbb{1}(g_{ij} \neq 0)$, i.e., if node j links to node i, $A_{ij} = 1$, 0 otherwise. The adjacency matrix is all we need to understand the connectivity in a network, but it contains less information than the coupling strength matrix as it does not tell us the coupling strengths associated with the connections. Therefore, in this project, $\mathbf{A}$ is less useful than $\mathbf{G}$.

To network scientists, the distribution of degrees and strengths are of particular interest as they are two high-level summaries of the connectivity of a network. Besides the basic summary statistics, e.g. mean, median and quantiles, the **probability distribution** of a measure is frequently looked at. Interestingly, for *real* networks such as a neuronal network, world wide web, human social network and marine food web, it is argued that the degree distribution follows a heavy- or long-tailed distribution; notably, for the social network, the distribution approximates a power law $P(k) \sim k^{-\gamma}$ [2]. This is an example of characteristics that happen to exist across different categories of networks. Is this a coincidence? This is an intriguing research topic in network science, and is nonetheless not the central subject to discuss here.

2.2 A Review – Network Reconstruction using Time Series

While it is never easy to directly unveil the network structure (the coupling strength matrix **G** is meant here), it is relatively easy to measure the dynamics of individual nodes, in the form of a collection of time series. There has been much ongoing research in search of methods that *reconstruct network links and coupling strengths from time series data*. Some ideas propose that we may infer links according to the correlations between the measured time series, with a larger correlation implying a higher probability of a link [3]. Some reconstruction methods make restrictive assumptions, which, for example, impose linearity or specific functional form on the dynamics [4]. These are not necessarily true, or are too good to be true, for real networks. *Below, a method that makes minimal assumptions proposed by Ching and Tam [5] is reviewed and presented.* The method extracts information about the network structure based on *a noise-induced relation* with loose assumptions. It assumes a highly generalizable form of network dynamics and makes no restriction on the dynamical functions. It is also shown that the method may be extended to high-dimensional systems, with each node carrying a vector of values instead of a single-valued state.

The method starts with a directed network of N nodes, with the state of each indicated by $x_i(t)$ where $i = 1, 2, ..., N$. The evolution of the dynamics of a node is composed of three components, namely (i) **intrinsic dynamics** $f_i(x_i)$, (ii) **nodal interaction** $h(x_i, x_j)$ and (iii) **noise** η_i. The dynamics of the whole network is governed by

$$\frac{\mathrm{d}x_i}{\mathrm{d}t} = f_i(x_i) + \sum_{j\neq i} g_{ij} h(x_i, x_j) + \eta_i \text{ where } i = 1, 2, ..., N. \tag{5}$$

Here, node j impacts node i via coupling function h, and the extent of the impact is tuned by coupling strength the g_{ij}. Typically, we assume $\partial h/\partial y > 0$ so that node j is **excitatory** if $g_{ij} > 0$ and **inhibitory** if $g_{ij} < 0$. If $g_{ij} = 0$, there is no link from node j to node i. This echoes our definition of excitatory and inhibitory edges discussed. External disturbances are summarized in η_i, modeled by a Gaussian white noise of zero mean: $\overline{\eta_i(t)\eta_j(t')} = D_{ij}\delta(t - t')$, where $\overline{\cdots}$ denotes an ensemble average over different realizations of the same system, and $\delta(\cdot)$ is the Dirac delta function. D_{ij} are the covariances between η_i and η_j, contained inside the noise covariance matrix **D**. *This is the prototype of a dynamical network, and different network models substitute a particular form of f_i and h.* To fully specify a network model, we need to supply the system of differential equations with *(1) coupling strength matrix* **G**, *(2) dynamical functions* $\{f_i\}_{i=1:N}$ *and* h, *and (3) noise covariance matrix* **D**. Given suitable initial conditions $\{x_i(t = 0)\}_{i=1:N}$, the system of equations can be numerically solved and $\{x_i(t)\}_{i=1:N}$ is the **network dynamics**.

The method targets systems that have stationary fluctuation around a **noise-free steady state**. Linearizing Eq. (5), we get

$$\frac{\mathrm{d}}{\mathrm{d}t}\delta\mathbf{x} \approx \mathbf{Q}\delta\mathbf{x} + \boldsymbol{\eta}, \tag{6}$$

where $\boldsymbol{\eta} = (\eta_1, ..., \eta_N)^T$, $\delta\mathbf{x} = (\delta x_1, ..., \delta x_N)^T$, and $\delta x_i = x_i - X_i$ is the deviation from the (constant) steady value X_i. Matrix **Q** contains information about the network and has entries

$$Q_{ij} = g_{ij} \left.\frac{\partial h(x, y)}{\partial y}\right|_{(X_i, X_j)} + \left[\sum_{k\neq i} g_{ik} \left.\frac{\partial h(x, y)}{\partial y}\right|_{(X_i, X_k)} + f_i'(X_i)\right] \delta_{ij}, \tag{7}$$

where only the first term remains for non-diagonal entries.

A (generalized) covariance matrix $\mathbf{B}(t_1, t_2)$ is defined:

$$\begin{aligned}\mathbf{B}(t_1,t_2) &\equiv \mathrm{Cov}(\mathbf{x}(t_1),\mathbf{x}(t_2)) \\ &\equiv \overline{\left[\mathbf{x}(t_1)-\overline{\mathbf{x}(t_1)}\right]\left[\mathbf{x}(t_2)-\overline{\mathbf{x}(t_2)}\right]^T} \\ &= \overline{\left[\delta\mathbf{x}(t_1)-\overline{\delta\mathbf{x}(t_1)}\right]\left[\delta\mathbf{x}(t_2)-\overline{\delta\mathbf{x}(t_2)}\right]^T},\end{aligned} \tag{8}$$

where the equality is because $X_i = \overline{X_i}$. $B_{ij}(t_1, t_2)$ encodes the covariance of measurements of node i at t_1 and node j at t_2.

As shown in the original paper [5], Eq. (6) can be solved to give

$$\mathbf{B}(t+\tau, t) \approx \exp(\tau\mathbf{Q})\mathbf{B}(t,t). \tag{9}$$

But a *stationary* dynamics is assumed, so $\mathbf{B}(t,t)$ is independent of t (i.e., the covariance matrix is time-independent) and $\mathbf{B}(t+\tau, t)$ depends on τ only (i.e., the lagged covariance matrix depends on the lag only). In practice, the ensemble average is approximated by the long time average,

$$\mathbf{B}(t+\tau,t) \approx \mathbf{K}_\tau \equiv \left\langle \left[\mathbf{x}(t+\tau) - \langle\mathbf{x}(t+\tau)\rangle\right]\left[\mathbf{x}(t) - \langle\mathbf{x}(t)\rangle\right]^T \right\rangle, \tag{10}$$

where $\langle\cdots\rangle$ denotes a time average. Then, Eq. (9) can be rewritten as

$$\exp(\tau\mathbf{Q}) \approx \mathbf{K}_\tau\mathbf{K}_0^{-1}, \tag{11}$$

where under a condition that $\tau \max_i |\,\mathrm{Im}(\lambda_i)| < \pi$, λ_i being the eigenvalues of $\mathbf{Q}$, $\mathbf{Q}$ can be retrieved:

$$\mathbf{Q} \approx \mathbf{M} \equiv \frac{1}{\tau}\log\left(\mathbf{K}_\tau\mathbf{K}_0^{-1}\right). \tag{12}$$

$\mathbf{M}$ can be computed from empirical time series of the nodes collected experimentally in some way while $\mathbf{Q}$ reflects the underlying model-based network structure. If we have time series that are sufficiently long, non-diagonal entries M_{ij} should compare well to Q_{ij}, i.e., $M_{ij} \approx Q_{ij} = g_{ij}\partial h/\partial y|_{(X_i,X_j)} \sim g_{ij}$ for $i \neq j$. Connectivity is estimated by separating M_{ij} into two groups: $g_{ij} \approx 0$ and $|g_{ij}| \gg 0$ using statistical techniques, e.g. Gaussian mixture model. Specifically, if M_{ij} is determined to be "near" zero, node i and node j are inferred to be unconnected; otherwise node j links to node i. Through clustering analysis, coupling strengths g_{ij} can be inferred too [5, 6]. Thus the method allows the reconstruction of network **links** and **coupling strengths** by using only the empirical time series data.

2.3 An Example Study

The method is verified in the following example, along with many other test cases in the original paper. The parameters are summarized as follows.

Type	Settings and Parameters
Network	Directed weighted random network (DWR) $N = 100$, connection probability $p = 0.2$, $g_{ij} \sim \mathcal{N}(10, 2)$
Dynamics	$(Intrinsic)$ $f_i(x) = r_i x(1-x), r_i = 10$ $(Interaction)$ $h^{\text{syn}}(x, y) = 1/\beta_1\{1 + \tanh[\beta_2(y - y_0)]\}$, $(\beta_1, \beta_2, y_0) = (2, 0.5, 4)$ $(Noise)$ $D_{ij} = \sigma_i^2 \delta_{ij}, \sigma_i = 1$
Initial Conditions	$x_i(t = 0) \sim \mathcal{U}[0, 5]$
Computational Settings	Step size $\delta t = 5 \times 10^{-4}$, time steps $N_{\text{data}} = 2 \times 10^6$

Table 1: Settings and parameters of the DWR network of 100 nodes for verifying the network reconstruction method reviewed.

$\mathcal{N}(\mu, \sigma)$ denotes a normal distribution of mean μ and standard deviation σ while $\mathcal{U}[a, b]$ denotes a uniform distribution over the sample interval $[a, b]$. The DWR network is randomly generated, with $\mathbf{G}$ produced using the following algorithm: (1) for all other nodes except node i, with probability p, assign an edge linking from the node to node i with a coupling strength sampled from $\mathcal{N}(\mu, \sigma)$, and (2) repeat for all $i = 1, 2, ..., N$. The choice of the *logistic* f_i as the intrinsic dynamics guarantees a stationary dynamics by providing a stable point of 1, which then permits the network reconstruction method. Nodal interaction h^{syn} adopts a *synaptic* form and works like a switch – if x_j passes the threshold y_0, this "triggers" x_i if node j links to node i. h^{syn} as a function of y takes a sigmoidal shape and tends to a step function for large β_2.

Eq. (5), the system of differential equations that governs the dynamics, is numerically solved using the *Euler-Maruyama algorithm* for N_{data} time steps to give a collection of N time series. The Euler-Maruyama algorithm is essentially the Euler algorithm, which iteratively applies a linear update to $x_i(t)$ by $x_i \leftarrow x_i + (\text{RHS}) \times \Delta t$, except that a noise term is added: $x_i \leftarrow x_i + (\text{RHS}) \times \Delta t + \sigma_i \epsilon \times \sqrt{\Delta t}$ where ϵ is a random number sampled from $\mathcal{N}(0, 1)$. RHS contains all the component terms of the rate of change. The noise-free time series, which have noise turned off ($\sigma_i = 0$), are also shown as a comparison. Time series of different nodes are labeled with different colors.

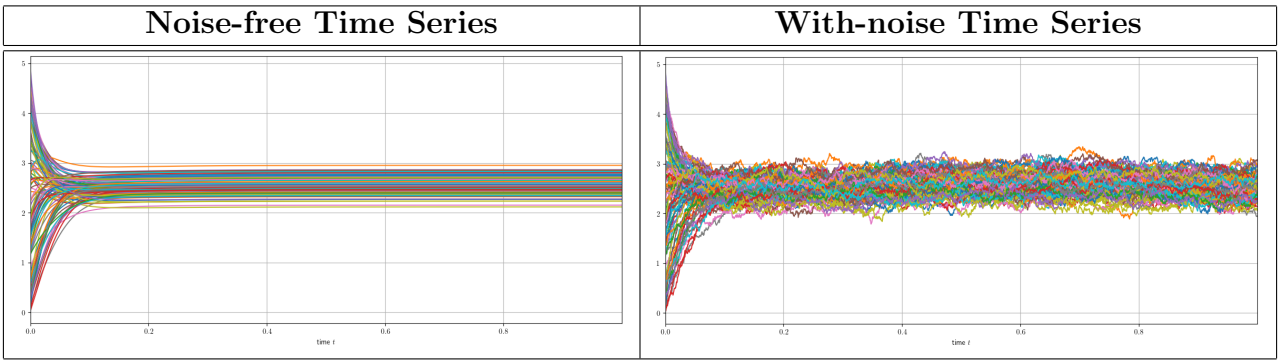

Figure 1: The noise-free and with-noise time series of the DWR network of 100 nodes. Time series of different nodes are labeled with different colors.

In the noise-free time series, the steady values X_i of the nodes cluster around 2 to 3 and we can see that they are lifted up away from the stable point of 1 in the logistic $f_i(x) = r_i x(1-x)$. In the

with-noise case, x_i fluctuate around their steady values but do not really cut the threshold $y_0 = 4$ in the synaptic h^{syn}. In later simulations, we attempt to choose a y_0 that approximates steady values in the hope that the crossing of threshold occurs more frequently.

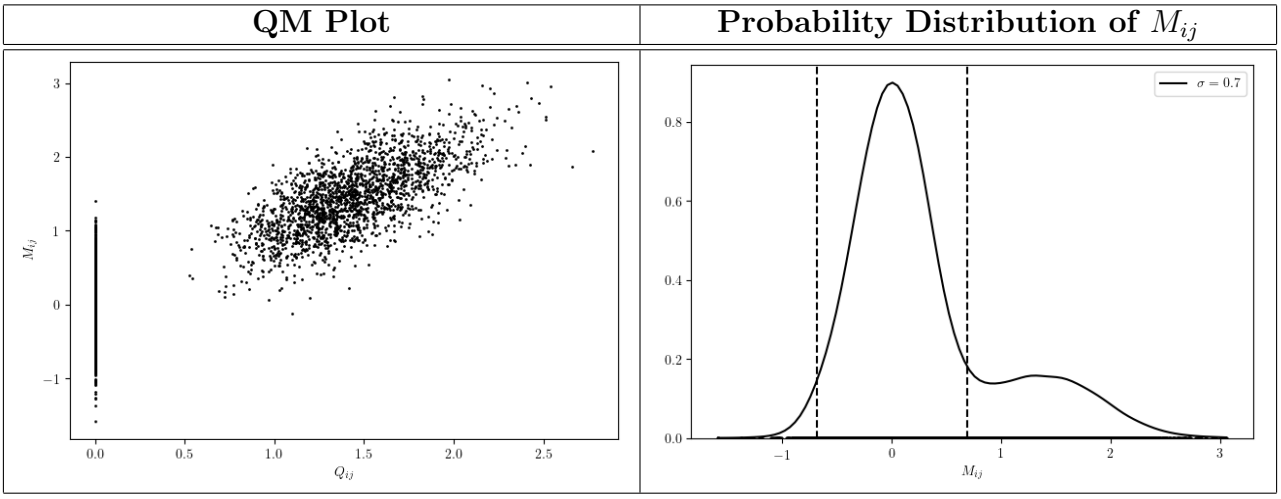

Figure 2: In the QM plot, the non-diagonal M_{ij} are plotted against Q_{ij}, with a linearity seen. In the probability distribution plot, M_{ij} have a distribution consisting of two merged Gaussians, one zero-centered, the other having a positive mean.

The non-diagonal M_{ij} are plotted against Q_{ij} in the QM plot. As predicted by Eq. (12), the linearity is clear. Because of the white noise inherent in the model, M_{ij} are subject to random fluctuations and this explains the vertical line of points at $Q_{ij} = 0$, which are centered around zero. The probability distribution of M_{ij} is given, and we see that the overall distribution may be fitted by a combination of two Gaussians, though with some degree of overlapping – one Gaussian is centered at zero while the other has a positive mean. Respectively, they correspond to the node pairs that are unlinked and linked, because $M_{ij} \approx 0$ implies $g_{ij} \approx 0$, hence the non-existence of link between the pair; non-zero M_{ij} implies otherwise. Notice that the zero-centered Gaussian has a peak that is nearly four times higher. This is due to the connection probability $p = 0.2$, causing 80% of node pairs to be unlinked and the remaining 20% to be linked, thus the ratio of 4. With, for example, the use of *Gaussian mixture model*, we know which Gaussian that each M_{ij} has a higher probability to belong to, thus recovering the linked pairs.

2.4 Empirical Network Data

The network reconstruction method has been applied to the empirical neuronal time series of cultures of rat embryonic cortices to estimate the coupling strengths g_{ij}, with the estimated links known as the **effective connectivity** [6]. The following dataset of estimated g_{ij} is provided by my supervisor and forms the foundation of later simulations in this project. The dataset takes the following format, where unstated node pairs are implied to be unconnected. Note again that g_{ij} is the coupling strength associated with the directed edge linking from node j to node i.

Node i	**Node** j	g_{ij}
1	196	0.0208720006
1	266	0.0156720001
1	267	0.0218959991
⋮	⋮	⋮
2	1	−0.0234200004
2	21	−0.00388139999
2	23	−0.00472760014
⋮	⋮	⋮
4095	4094	0.0089673996

Table 2: The dataset of the reconstructed coupling strengths g_{ij} based on the empirical neuronal time series data.

There are collectively $64 \times 64 - 1 = 4095$ electrodes to measure electrical signals of the rat embryonic neurons, hence the neuronal network contains 4095 nodes. Precisely speaking, the nodes are not actually the neurons, but the electrodes serving as proxy for the "underlying" neurons. This approach is used because, experimentally, it is difficult to pinpoint a particular neuron. The network is sparse – only a tiny fraction (1.4%) of all possible node pairs are linked. Coupling strengths of the excitatory and inhibitory edges, i.e., $\{g_{ij} : g_{ij} > 0\}$ and $\{|g_{ij}| : g_{ij} < 0\}$, are discovered to exhibit a long-tailed distribution. This echoes with literatures. For example, it is well known to network scientists that biological parameters, e.g. neuron firing rate and synaptic weights, have long, heavy tails and are highly skewed [7, 8]. This is in contrast with the common belief in the past that brain parameters obey bell-shaped distributions and, therefore, biologists often rely on *mean* and *standard deviation* to understand the data. This is inadequate for describing data that have *a long tail* because the degree of dispersion is not comprehensively summarized by the standard deviation and the mean is also subject to heavy influence of the extreme outliers. In this case, higher-order moments and quantiles are relatively useful. This will be further discussed.

Neuronal spiking dynamics are *highly skewed* and *long-tailed*. Here, we analyze the spike distribution based on the following dataset of rat embryonic neuronal spike counts after 25 days in vitro, provided by my supervisor.

Node i	**Spike Count**
1	521
2	9
3	6
⋮	⋮
4095	11

Table 3: The dataset of the rat embryonic neuronal spike counts after 25 days in vitro.

The spike counts form the following probability distribution plots.

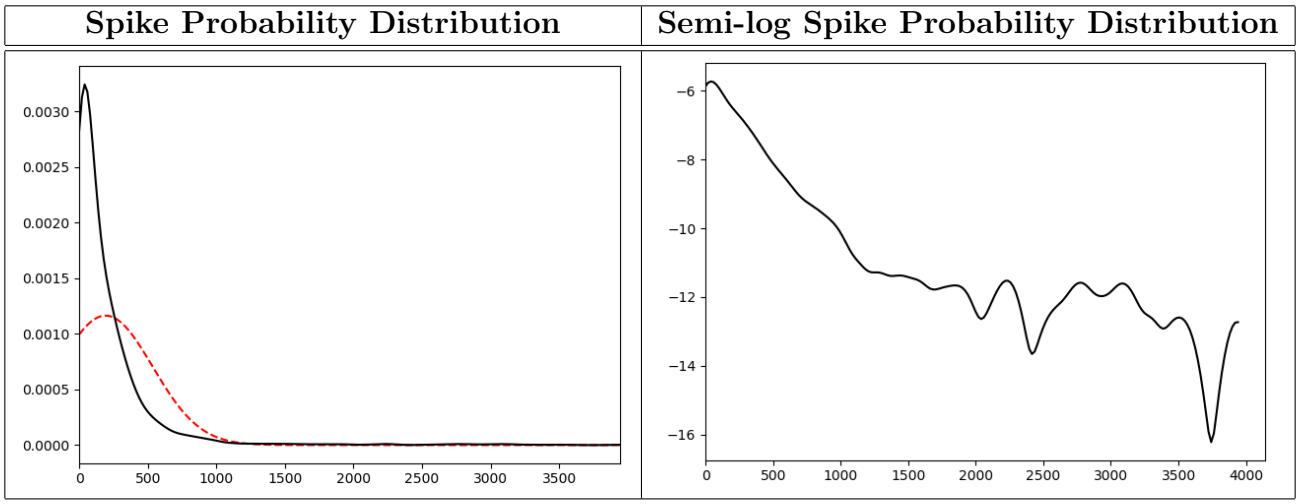

Figure 3: In the spike probability distribution plot, the curve is seen to have a long right tail. The Gaussian (red dashed line) with the same mean and standard deviation is shown as comparison. In the semi-log plot, a linearity is seen for small spike counts while there are fluctuations for large spike counts.

Distribution	Mean	Standard Deviation	Skewness	Excess Kurtosis
Gaussian	192.32	342.84	0	0
Spike	192.32	342.84	5.39	39.08

Table 4: The first four moments of the spike counts and the Gaussian with the same mean and standard deviation.

The histogram of the spike counts is normalized and smoothed using kernel techniques (with the `scipy.stats.gaussian_kde` in the SciPy library of Python) to give the spike probability distribution curve. The probability distribution is compared to a Gaussian (red dashed line) that has the same mean (192.32) and standard deviation (342.84). It can be seen from the plot that the probability distribution has a peak value three times as high as that of the Gaussian and a tail extending far to the right. The x-axis stops at the largest value of spike count (3941).

The table shows the first four moments of the Gaussian and the spike probability distribution, where the skewness and the excess kurtosis are respectively given by

$$\text{Skew.} = \frac{\overline{(X-\mu)^3}}{\sigma^3} \text{ and Excess Kurt.} = \frac{\overline{(X-\mu)^4}}{\sigma^4} - 3, \tag{13}$$

with μ being the mean and σ being the standard deviation of the data. For a Gaussian, the skewness and the excess kurtosis are both zero. Unlike standard deviation, skewness and kurtosis are scale-free measures that can be compared across different datasets. The positive skewness implies that the distribution is *right-skewed* with a mean greater than the median and the large kurtosis implies that it has a *significantly longer tail* than the Gaussian.

While a large majority of nodes have spike counts fewer than 100, there are 14 nodes with spike counts larger than 3000, which are *8 standard deviations* from the mean. This would be practically impossible if spike counts were to obey a normal distribution because, at 8 standard deviations, the probability density would take an order of 10^{-15}, requiring on average 10^{15} nodes to have one such occurrence. Nevertheless, in our sample that comprises only 4095 nodes, there are already 14 occurrences! The extreme outliers again indicate that the distribution has a long, heavy tail.

The *exponential distribution* is one candidate to model a long/heavy-tailed distribution. In the semi-log plot, we take logarithm on the probability density to examine how well it may be approximated by an exponential distribution, which theoretically has the form $P(x) = \lambda e^{-\lambda x}$ and logarithm gives $\log P(x) = \log \lambda - \lambda x$ (linear). We can see that for the nodes with spike counts fewer than 1000, there is a clear linearity but there are a lot of fluctuations for nodes with greater spike counts. Although nodes with large spike counts do exist, the number is significantly smaller, subjecting the line fit to statistical noise. It is hard to draw a conclusion on the nature of the distribution for the large-spike nodes. *But for the low-spike nodes, we can conclude that the distribution is well approximated by an exponential distribution.*

To summarize, the empirical rat embryonic spike counts have the following characteristics: *highly right-skewed, long-tailed and have very extreme outliers.* A good neuronal network model should be able to generate time series that are successful in recovering these spike characteristics.

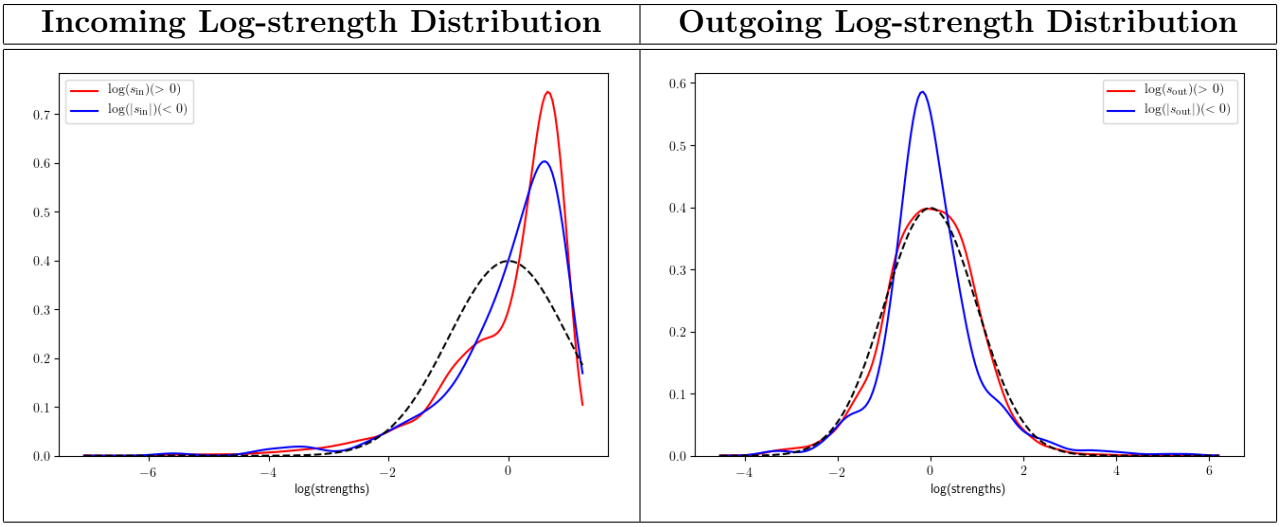

Figure 4: The probability distribution of the standardized incoming and outgoing log-strengths. Both are seen to have a long tail extending to 6 standard deviations from the mean.

Like the neuronal spikes, the incoming and outgoing strengths $s_{\text{in/out}}(i)$ derived from the coupling strengths g_{ij} (extracted using the network reconstruction method discussed) are also long-tailed. The plots show the probability distributions of the standardized incoming and outgoing log-strengths compared to a standard Gaussian (black dashed line). Note that to *standardize* a dataset $\{X_i\}$, the data are transformed according to $X_i \to (X_i - \mu)/\sigma$, where μ and σ are respectively the mean and standard deviation.

The in/out-strengths are both grouped into two classes according to the signs. For both the in- and out-strengths, the tails are long and, to convert the values to a more reasonable scale, logarithms are taken. For the incoming log-strengths, we can see that the probability distribution is left-skewed with a long left tail. For the outgoing log-strengths, the probability distribution is relatively symmetric, and the positive strength class is well approximated by a Gaussian while the negative strength class has a thinner but taller peak. For both in- and out-strengths, there are outliers at over 6 standard deviations from the mean.

Motivation. We can see that both the neuronal spike distribution and the in/out-strength distribution are *skewed* and have *a long tail*. A natural question one may raise is: *Does the distribution of synaptic strength have an effect on the spiking dynamics? If it does, how does the spiking dynamics correlate with the synaptic strengths?* This is the central question this project aims to address.

2.5 Classes of Dynamical Functions

What vary across different network models are *merely* the dynamical functions to be substituted, including the *intrinsic dynamics* $\{f_i(x)\}_{i=1:N}$ (with the argument being x_i) and the *nodal interaction* $h(x, y)$ (with the arguments being x_i, x_j). These are the standard functional inputs to a one-dimensional network model with each node carrying a single-valued state. However, for a high-dimensional network model, the FitzHugh-Nagumo (FHN) model for example, the intrinsic dynamics may be extended to $\{f_i^x(x, y), f_i^y(x, y)\}_{i=1:N}$ (with the argument being x_i, y_i). Simulations in this project are entirely based on the following two intrinsic dynamics functions combined with the two nodal interaction functions, given in the table. With the reconstructed coupling strength matrix $\mathbf{G}$, the dynamics of the *giant* neuronal network consisting of 4095 nodes are solved, under the assumption of different combinations of trial intrinsic dynamics and nodal interaction.

To summarize, a one-dimensional network model is governed by

$$\frac{\mathrm{d}x_i}{\mathrm{d}t} = f_i(x_i) + \sum_{j\neq i} g_{ij} h(x_i, x_j) + \eta_i \text{ where } i = 1, 2, ..., N, \qquad \text{(One-dimensional)}$$

while a two-dimensional network model is governed by

$$\begin{aligned} \frac{\mathrm{d}x_i}{\mathrm{d}t} &= f_i^x(x_i, y_i) + \sum_{j\neq i} g_{ij} h(x_i, x_j) + \eta_i \qquad \text{(Two-dimensional)} \\ \frac{\mathrm{d}y_i}{\mathrm{d}t} &= f_i^y(x_i, y_i) + G \text{ where } i = 1, 2, ..., N, \end{aligned}$$

where G collects the nodal interaction and the noise term. In this project, $G \equiv 0$ for two-dimensional models.

Intrinsic Dynamics $\{f_i(x)/f_i^{x/y}(x, y)\}_{i=1:N}$	**Nodal Interaction** $h(x, y)$
(*Logistic*) $f_i(x) = r_i x(1 - x)$ Parameters: $\{r_i\}$	(*Diffusive*) $h^{\mathrm{diff}}(x, y) = y - x$ Parameters: None
(*FitzHugh-Nagumo*) $f_i^x(x, y) = (x - x^3/3 - y)/\epsilon$ $f_i^y(x, y) = x + \alpha$ Parameters: $\{\epsilon, \alpha\}$	(*Synaptic*) $h^{\mathrm{syn}}(x, y) = 1/\beta_1\{1 + \tanh[\beta_2(y - y_0)]\}$ Parameters: $\{\beta_1, \beta_2, y_0\}$

Table 5: The functional forms of the intrinsic dynamics, namely logistic and FitzHugh-Nagumo (FHN), and the nodal interaction, namely diffusive and synaptic, used in this project.

For the nodal interaction, both the diffusive and synaptic functional form are physically well-justified choices.

(1) (*Synaptic*) When x_j breaches y_0, h^{syn} is triggered, acting like a switch. It plays precisely the role of the *activation function* in a neuron – a neuron fires and gives a spiking electrical signal when its membrane potential exceeds a certain threshold. With the choice of h^{syn} and a y_0 designed to be close to the steady values X_i, *possibly* neuronal spiking activity can be recovered. The following mechanism is expected to happen. When node j spikes and, at some instant, takes a very large value breaching the threshold, neuron i that it links to responds to the triggered h^{syn} by taking a large instantaneous rate of change (assuming that the directed edge takes a positive coupling strength g_{ij}). In turn, this affects the neurons that neuron i links to, and a ripple effect can *possibly* be induced – a group of linking neurons spike simultaneously.

(2) (*Diffusive*) When neuron j spikes and, at some instant, takes a very large value, neuron i that it links to takes a large instantaneous rate of change due to the large h^{diff} interaction term (again, assuming a positive g_{ij}). x_i evolves in such a way as to equalize x_i and x_j because, when $x_i \approx x_j$, $h^{\text{diff}}(x_i, x_j) \approx 0$, making a negligible contribution to the nodal interaction term, hence slowing down the rate of change. Ripple effect *possibly* causes spikes to spread to other neurons.

The word "*possibly*" is stressed because these are only our intuitive understanding (or guess) of the effects of the nodal interaction term. *Does it actually work in the way we expect?* In fact, the *intrinsic dynamics* also has an important role to play when it comes to spiking dynamics. In the later simulations, we will see that spiking dynamics is not apparent in the logistic network model, which has logistic $\{f_i(x)\}$, and, in contrast, quite well-defined in the FHN network model, which has FHN $\{f_i^{x/y}(x, y)\}$.

Model Overview. The project tests two models, each obeying a different intrinsic dynamics.

(1) (*Logistic Intrinsic Dynamics – Failed*) Built upon the reconstructed coupling strength matrix $\mathbf{G}$, the model neuronal time series are generated by numerically solving Eq. (5) under the assumption of a *logistic* intrinsic dynamics $\{f_i\}$ and a *diffusive* as well as *synaptic* nodal interaction h. (The different classes of dynamical functions will be summarized at the end of this section.) Then, the spiking dynamics are respectively analyzed. *This, however, is a vain attempt to represent the neurons.*

(2) (*FHN Intrinsic Dynamics – Improved*) Adopting a similar procedure, the model neuronal time series are generated under the assumption of a *FitzHugh-Nagumo* (FHN) intrinsic dynamics $\{f_i\}$ and a *diffusive* as well as *synaptic* nodal interaction h. In the FHN model, the neurons take two-dimensional states $(x_i(t), y_i(t))$, and with this model, *the generated time series are significantly more realistic and the spiking dynamics exhibit certain features that are empirically observed.* Network features that potentially drive the spiking dynamics are studied.

3 Analysis of the Logistic Network Model

The logistic intrinsic dynamics ensures mean reversion and tends to stabilize the dynamics. If, due to spiking at some instant, the state of a node jumps to a very large value, in the time steps that follow, the state then experiences a large tendency to revert back to a smaller value, for now $f_i(x_i) = r_i x_i(1 - x_i)$ becomes very negative.

With the reconstructed coupling strength matrix $\mathbf{G}$ of the 4095 nodes representing the neurons, Eq. (5) that governs the dynamics is numerically solved. In this section, a *logistic* intrinsic dynamics is assumed, and, for the nodal interaction, the *synaptic* as well as *diffusive* functional form are attempted. The behavior of such a non-random giant network with heavy-tailed synaptic strengths is not at all obvious, and not in any way comparable to the simple directed Gaussian-weighted random network of 100 nodes discussed in the introduction. Lacking theories to assist in our understanding of the dynamics, at the current stage, running the simulation is the sole way to probe into its properties. Inspecting the dynamics, both models are doing a poor job of generating realistic neuronal spiking dynamics. The model-generated time series are discussed below, and we will see *how the assumption of a logistic intrinsic dynamics is a failed attempt.*

3.1 Synaptic Nodal Interaction

Assuming a synaptic nodal interaction term, a simulation with the following tabulated set of parameters is run.

Type	**Settings and Parameters**
Network	Based on the reconstructed coupling strength matrix $\mathbf{G}$ ($N = 4095$)
Dynamics	(*Intrinsic*) $f_i(x) = r_i x(1-x), r_i = 100$ (*Interaction*) $h^{\text{syn}}(x,y) = 1/\beta_1\{1+\tanh[\beta_2(y-y_0)]\}$, $(\beta_1, \beta_2, y_0) = (2, 0.5, 1)$ (*Noise*) $D_{ij} = \sigma_i^2 \delta_{ij}, \sigma_i = 0.5$
Initial Conditions	$x_i(t=0) \sim \mathcal{U}[0.9, 1.1]$
Computational Settings	Step size $\delta t = 5 \times 10^{-4}$, time steps $N_{\text{data}} = 2 \times 10^6$

Table 6: Settings and parameters of the logistic network model with the synaptic nodal interaction.

The noise-free time series, which have noise turned off ($\sigma_i = 0$), are shown, with different nodes labeled with different colors. For the with-noise time series, for clarity, two specific nodes are selected, and their states are seen to fluctuate around their respective steady values, indicated by the horizontal dashed lines. Note that the noise-free time series reach their stationary states at $t = 1$ approximately, after experiencing the initial transient states. Roughly, the stationary states lie in the interval $[0.9, 1.1]$, which are centered around the stable point 1 of the logistic intrinsic dynamics $f_i(x) = r_i x(1-x)$. For the with-noise time series, therefore, we choose to look at the time interval $[160, 162]$ to ensure that the non-stationary transient effects have vanished.

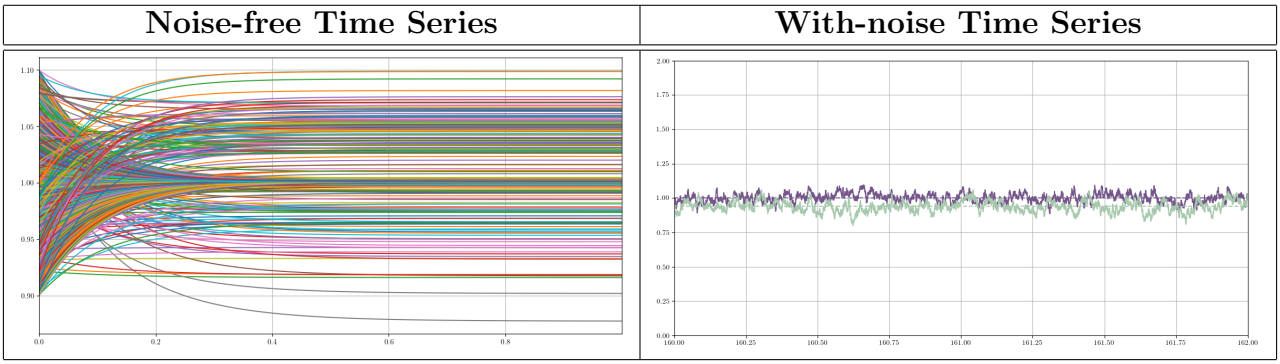

Figure 5: The noise-free and with-noise time series of the logistic network model with the synaptic nodal interaction. Time series of different nodes are labeled with different colors.

Looking at the with-noise time series, spikes are not apparent, and are not in the shape we would expect for neuronal spikes. Rather, in my view, it is more appropriate to recognize them as *fluctuations* instead of *spikes*. While not shown here, several other sets of parameters, with other trial $r_i, (\beta_1, \beta_2, y_0), \sigma_i$, are tested and, still, no apparent spike is observed. *It is therefore concluded that this logistic network model combined with a synaptic nodal dynamics does not have a good performance in producing neuronal spikes.*

3.2 Diffusive Nodal Interaction

Assuming a diffusive nodal interaction term, a simulation with the following tabulated set of parameters is run.

Type	**Settings and Parameters**
Network	Based on the reconstructed coupling strength matrix $\mathbf{G}$ ($N = 4095$) (*Modification*) Coupling strengths g_{ij} rescaled by 10
Dynamics	(*Intrinsic*) $f_i(x) = r_i x(1-x), r_i = 10$ (*Interaction*) $h^{\text{diff}}(x,y) = y - x$ (*Noise*) $D_{ij} = \sigma_i^2 \delta_{ij}, \sigma_i = 0.25$
Initial Conditions	$x_i(t=0) \sim \mathcal{U}[0.9, 1.1]$
Computational Settings	Step size $\delta t = 5 \times 10^{-4}$, time steps $N_{\text{data}} = 2 \times 10^6$

Table 7: Settings and parameters of the logistic network model with the diffusive nodal interaction.

The noise-free time series, which have noise turned off ($\sigma_i = 0$), are shown, with different nodes labeled with different colors. For the with-noise time series, for clarity, two specific nodes are selected, and their states are seen to fluctuate around their respective steady values, indicated by the horizontal dashed lines. Note that the noise-free time series reach their stationary states at $t = 1$ approximately, after experiencing the initial transient states. Here, interestingly, all stationary states are identically 1, corresponding to the stable point of the intrinsic dynamics $f_i(x) = r_i x(1-x)$. This is not hard to understand – in Eq. (5), $x_i(t) \equiv 1$ for all i is the trivial solution. For the with-noise time series, again, we choose to look at a later time interval $[200, 202]$ to ensure that the non-stationary transient effects have vanished.

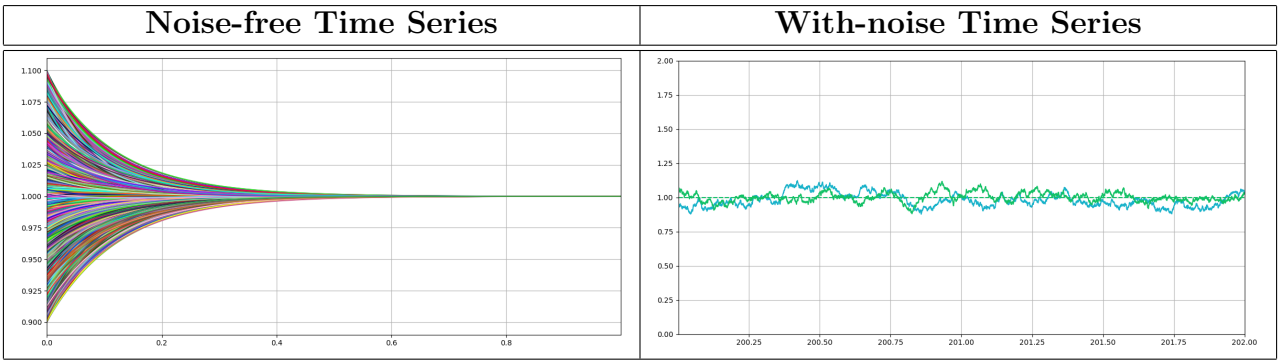

Figure 6: The noise-free and with-noise time series of the logistic network model with the diffusive nodal interaction. Time series of different nodes are labeled with different colors.

Looking at the with-noise time series, as with the synaptic nodal dynamics, spikes are not apparent, and are not in the shape we would expect for neuronal spikes. Rather, in my view, it is more appropriate to recognize them as *fluctuations* instead of *spikes*. While not shown here, several other sets of parameters, with other trial r_i, σ_i, are tested and, still, no apparent spike is observed. *It is therefore concluded that this logistic network model combined with a diffusive nodal dynamics does not have a good performance in producing neuronal spikes.*

Degree and *strength* are two summary statistics to understand the "connections" in a network. It is not unnatural to assume that they are associated in some way with the dynamics. As spikes are not well produced in this model, for the dynamics, we choose to look at the standard deviation of the fluctuations in the time series. *Do the in-degrees and in-strengths correlate in any way with the time*

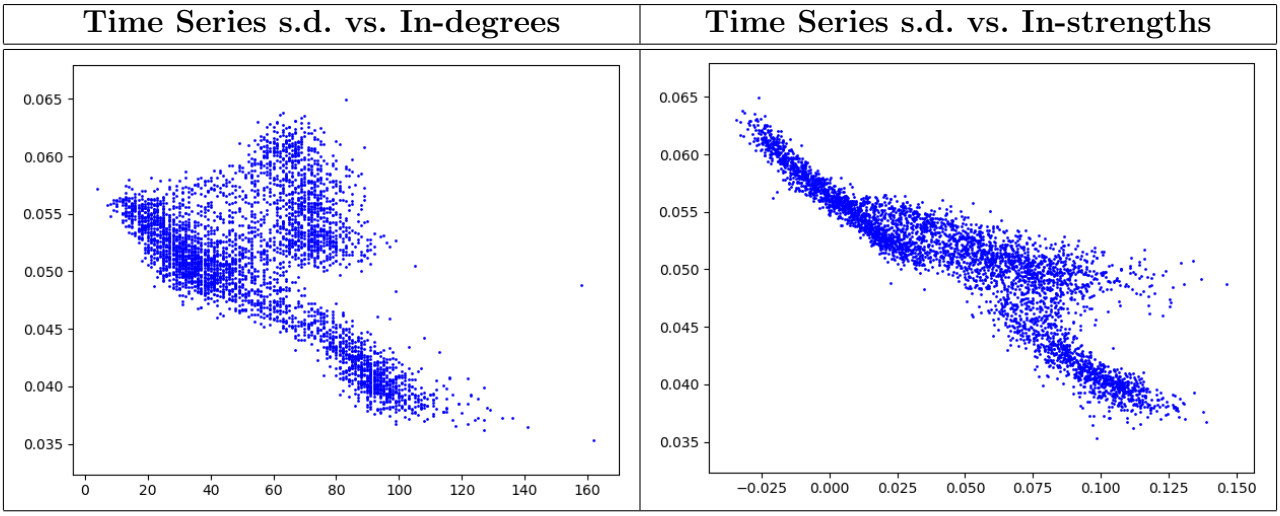

Figure 7: The negative relations of the time series s.d.'s with the in-degrees and in-strengths.

series standard deviations? The time series s.d.'s are computed over the N_{data} time steps for each node, and the in-degrees as well as the in-strengths are derived based on the reconstructed coupling strength matrix $\mathbf{G}$. It is seen that there exist negative relations. From the plots, the overall trend is that the s.d.'s decrease with both in-degrees and in-strengths. In other words, the more nodes linking to a specific node and the more positive the linking coupling strengths are, the more "stable" the time series of that node is. *It is therefore concluded that positive nodal connections (i.e., positive g_{ij}) tend to stabilize the dynamics.* But a caveat is that the conclusion is specific to this particular logistic network model with a diffusive nodal dynamics, and there is no reason to assume that this generalizes to other sorts of dynamics.

While not shown here, similar analysis is performed for the *out-degrees* and *out-strengths*, but it is seen to contain no obvious trend. *Thus, in-measures have a more direct and apparent effect on the dynamics than out-measures.* Tracing back to Eq. (5), this actually makes much sense as the rate of change of a state x_i is driven by the incoming coupling strengths g_{ij}, out of which the in-measures are derived.

4 Analysis of the FHN Network Model

The FitzHugh–Nagumo (FHN) model describes the dynamics of an excitable system, such as a neuron, and is a simplified two-dimensional version of the Hodgkin–Huxley model, which describes the initiation and propagation of the action potentials in spiking neurons. In this section, the FHN dynamical functions are incorporated into the intrinsic dynamics in Eq. (5) with the extension that each node carries a two-dimensional state $(x_i(t), y_i(t))$. As discussed in the introduction, the two-dimensional network model, upon the substitution of the FHN dynamical functions, is given by

$$\frac{\mathrm{d}x_i}{\mathrm{d}t} = \frac{1}{\epsilon}\left(x_i - \frac{x_i^3}{3} - y_i\right) + \sum_{j\neq i} g_{ij} h(x_i, x_j) + \eta_i \tag{14}$$

$$\frac{\mathrm{d}y_i}{\mathrm{d}t} = x_i + \alpha \text{ where } i = 1, 2, ..., N, \tag{15}$$

with parameters $\epsilon, \alpha \geq 0$. With the reconstructed coupling strength matrix $\mathbf{G}$ of the 4095 nodes representing the neurons, this set of $2N$ differential equations that governs the dynamics is numerically solved. In this section, an *FHN* intrinsic dynamics is assumed, and, for the nodal interaction, the *diffusive* as well as *synaptic* functional form are attempted.

Before running simulations on the giant neuronal network, parameter testing is performed on *a small DWR network of 100 nodes*, which has exactly the same network settings as the example in the introduction with $\sigma_i = 1$ for the noise, in order to better understand how different combinations of (ϵ, α) affect the dynamics. For simplicity, a *diffusive* nodal interaction term h^{diff}, which has no parameter, is assumed.

The effects of ϵ and α are separately studied. Each set of (ϵ, α) represents a different FHN network model, on which a simulation is run and time series of the 100 nodes over the time interval $[0, 10]$ are returned. With α fixed to 0.95, ϵ is varied, taking values of $0.01, 0.1, 1, 10$. At $\epsilon = 0.01$, the spikes are "solid", with clear-cut excitation and relaxation. Prior to a spike, the time series are on an upward trend and, upon passing a certain trigger point, a simultaneous spiking of the 100 nodes is induced. Then, the spikes quickly relax to the initial starting point at -2. *This is precisely the pattern one would expect to see in a neuronal spiking dynamics.* We can see also that the spikes are periodic, and that there is no ambiguity between *spikes* and *fluctuations*, which have very different time scales. At $\epsilon = 0.1$, spikes are less sharp and, still, they are well-defined and periodic. But with larger ϵ, spikes are no longer clear and they smooth to become oscillations – they are not sharp enough to be recognized as spikes. Also, the time scale of a spike lengthens and, in particular, at $\epsilon = 10$, we can barely see a complete cycle of spiking dynamics. *Therefore, it is concluded that smaller ϵ leads to sharper and shorter spikes that are more well-defined.* This can be physically understood as follows. In Eq. (14), the FHN term controls the spiking dynamics and the nodal interaction term controls the correlations between the dynamics of the linking nodes. A small ϵ causes the FHN term to be dominant, hence a clearer spiking pattern.

To understand the effect of α, ϵ is fixed to 0.01 and α is varied, taking values of $0, 0.95, 1, 1.05$. At $\alpha = 0$, the time series are symmetric about 0, with the spike parts indistinguishable from the non-spike parts except for a reflection. The dynamics is also perfectly periodic. The $\alpha = 0.95$ case was discussed, and this is a sensible model to produce neuronal spiking dynamics. At $\alpha = 1$, there is no apparent difference compared to the $\alpha = 0.95$ case, but when α is tuned past 1, the dynamics critically smooths and has entirely no spike except for the initial transient spike. $\alpha = 1$ *is a critical threshold beyond which no spiking dynamics can be observed.*

The parameter testing hints that sets of parameters (ϵ, α) *with* $\epsilon \sim 0.01$ *to* 0.1 *and* $\alpha \sim 0.95$ *in the*

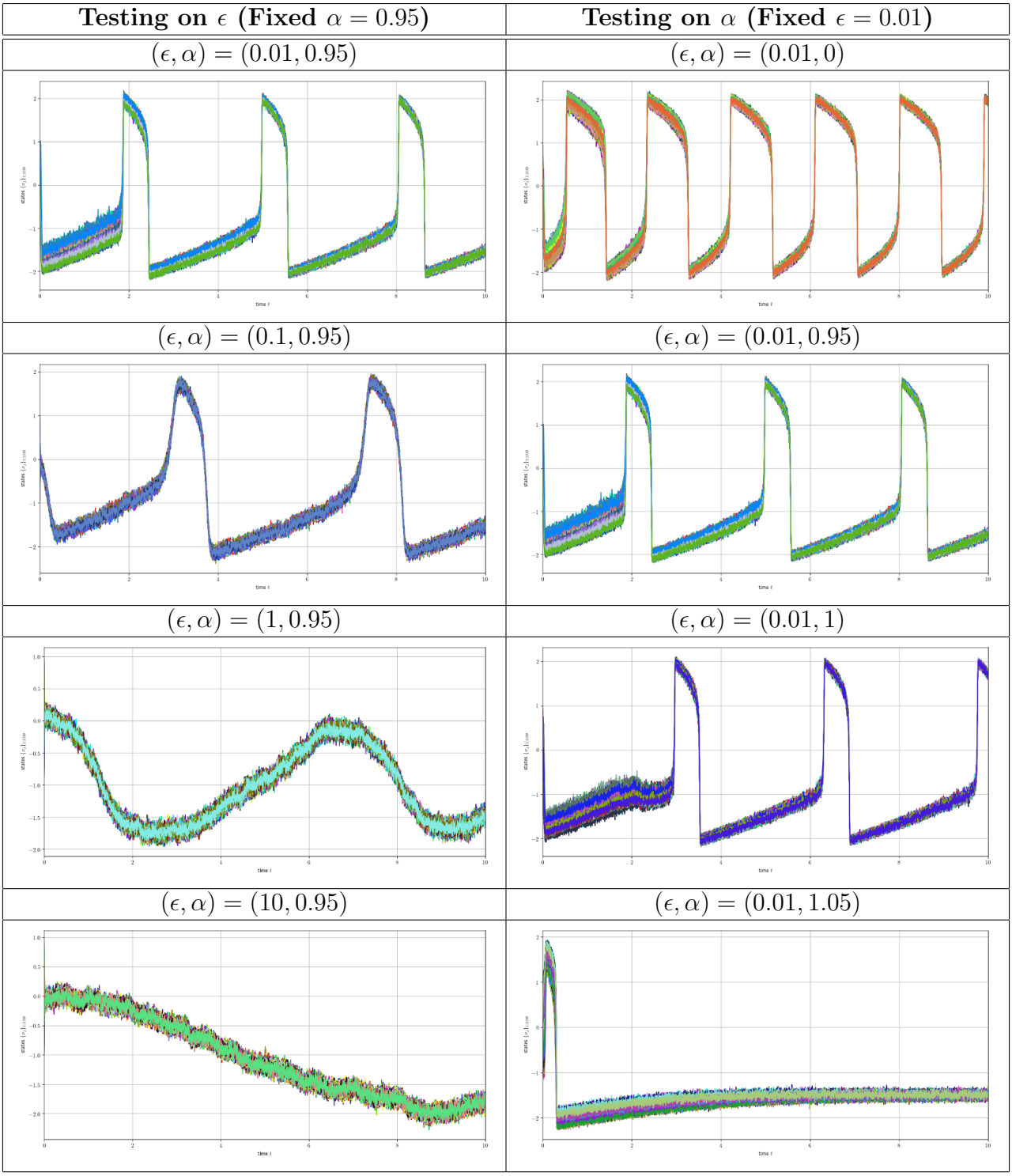

Figure 8: Parameter testing on the FHN network model using the DWR network of 100 nodes.

FHN term are good at producing realistic neuronal spiking dynamics. Later simulations, which run on the giant reconstructed network of 4095 nodes, follow this conclusion.

Now we can see that the FHN term works well for the DWR network of 100 nodes. For our gigantic non-random neuronal network, does it still work properly? I am thankful that it does. In the following parts, the FHN dynamical function is applied to our reconstructed $\mathbf{G}$ and the behavior of the neuronal spikes, under the assumption of the *diffusive* as well as *synaptic* nodal interaction, is studied.

4.1 Diffusive Nodal Interaction

The *FHN* network models combined with the *diffusive* nodal interaction h^{diff} and using the following sets of parameters are investigated. For all models thereafter, $\sigma_i = 2$ is consistently used for the noise.

- (*Case 1*) $(\epsilon, \alpha) = (0.1, 0.95)$
- (*Case 2*) $(\epsilon, \alpha) = (0.01, 0.95)$
- (*Case 3*) $(\epsilon, \alpha) = (0.1, 1)$
- (*Case 4*) $(\epsilon, \alpha) = (0.1, 1.05)$

Type	**Settings and Parameters**
Network	Based on the reconstructed coupling strength matrix $\mathbf{G}$ $(N = 4095)$
Dynamics	(*Intrinsic*) $f_i^x(x, y) = (x - x^3/3 - y)/\epsilon, f_i^y(x, y) = x + \alpha$ (*Interaction*) $h^{\text{diff}}(x, y) = y - x$ (*Noise*) $D_{ij} = \sigma_i^2 \delta_{ij}, \sigma_i = 2$
Initial Conditions	$x_i(t = 0) \sim \mathcal{U}[-1, 1]$
Computational Settings	Step size $\delta t = 5 \times 10^{-4}$, time steps $N_{\text{data}} = 2 \times 10^6$

Table 8: Settings and parameters of the FHN network model with the diffusive nodal interaction.

To see how the models are behaving, both the noise-free and with-noise time series of node 0 over the time interval $[0, 50]$ are inspected. The spikes are selected using the peak detection algorithm (`scipy.signal.find_peaks`) in the SciPy library of Python, and are labeled with red crosses. There are two additional conditions to ensure that the spikes determined are indeed what we would expect if we were to do the job manually: *spikes have to (1) lie above $h = 0$, and (2) be at least separated by $d = 2000$ time steps.* The conditions make sure that the selected spikes are "sufficiently tall" and avoid the over-counting of spikes that actually "belong to the same spike". Following the algorithm, the time series together with the selected spikes are shown.

In Case 1, spikes are apparent in the noise-free time series of node 0. While, initially, the spikes are irregular and differ in shape, after the transient period stopping at $t = 20$ approximately, the spikes are identical in shape. When the noise of $\sigma_i = 2$ is turned on, the periodic pattern is disrupted, and we can see in the with-noise time series that the time separations between spikes are irregular. The spikes also have differing heights, although a majority of them lie above 2. The positions of the spikes in the with-noise time series roughly correspond to that in the noise-free time series. In Case 2, which has an ϵ ten times smaller, the with-noise time series are apparently "cleaner" and more periodic. In fact, this echoes our previous conclusion that smaller ϵ leads to a dominant FHN term, hence the obvious spiking pattern. Notice also that spikes are denser, compared to Case 1.

In Case 3, α lies at the threshold of 1, and the noise-free time series is seen to have a tiny oscillation around the level of -1 but no obvious spike, except the initial transient one, can be found. Nonetheless, in the with-noise time series, the noisy spiking pattern as in Case 1 is seen. Likewise, in Case 4, while the noise-free time series is boring, lacking any spiking pattern, when noise is turned on, the noisy spiking pattern as in Case 1 emerges. This is unexpected as, in reference to the small DWR network discussed, $\alpha > 1$ gives no spike at all. But here, in Case 4, the spiking pattern is actually very active! This is a non-trivial aspect of large network dynamics – *results that apply to small networks do not necessarily work for large networks.*

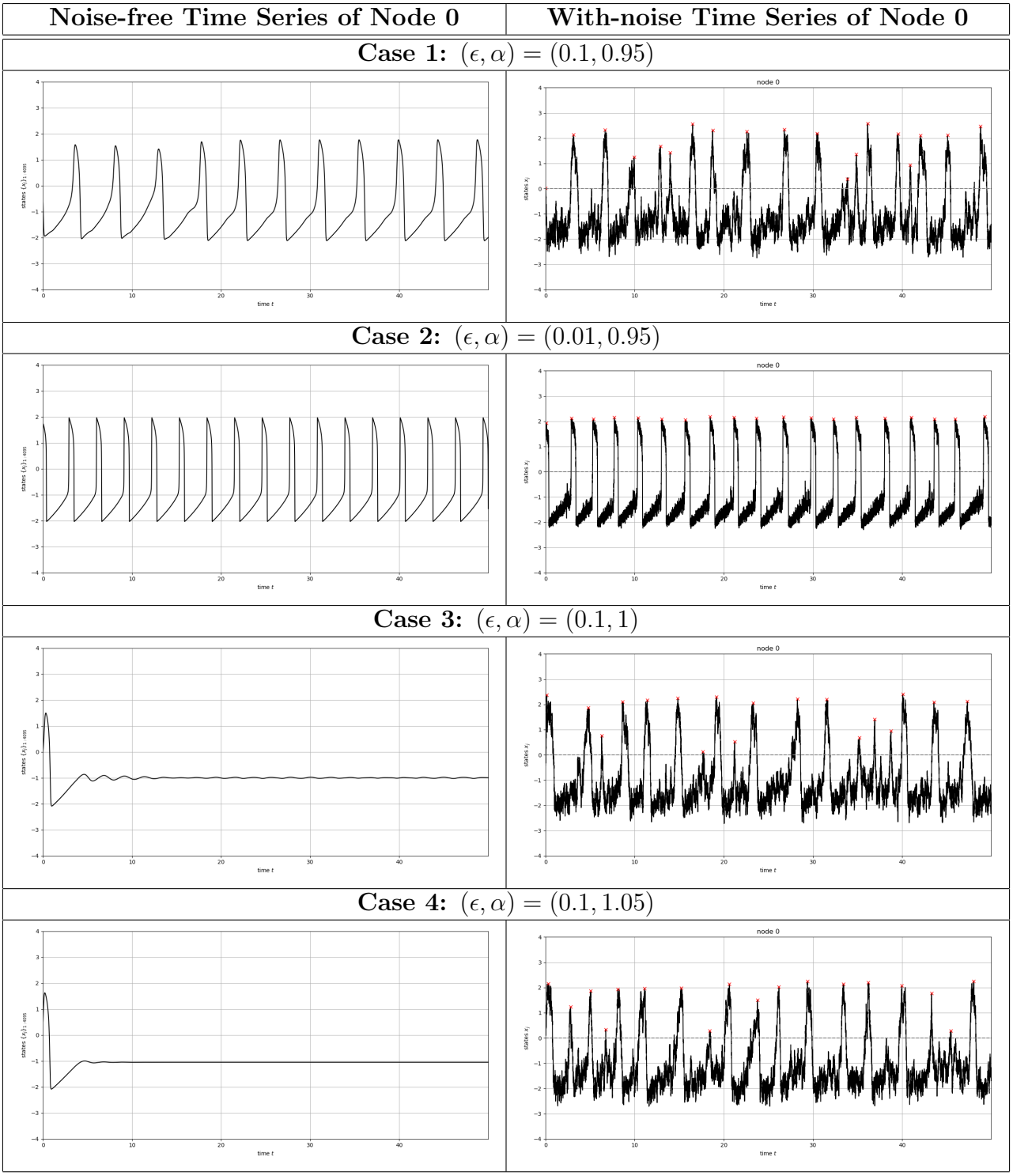

Figure 9: Parameter testing on the FHN network model with the diffusive nodal interaction.

4.1.1 Spike Probability Distribution

As the time series in Case 2 are too ordered and periodic, we choose to exclude Case 2. The time series in Case 1, 3 and 4 *look* realistic, *but are they?* Recall from the introduction that the empirical rat embryonic spike counts have the following characteristics: *highly right-skewed, long-tailed and have very extreme outliers.* Here, we look into the probability distribution of the standardized spike counts and compare Case 1, 3 and 4 in terms of quantiles and moments.

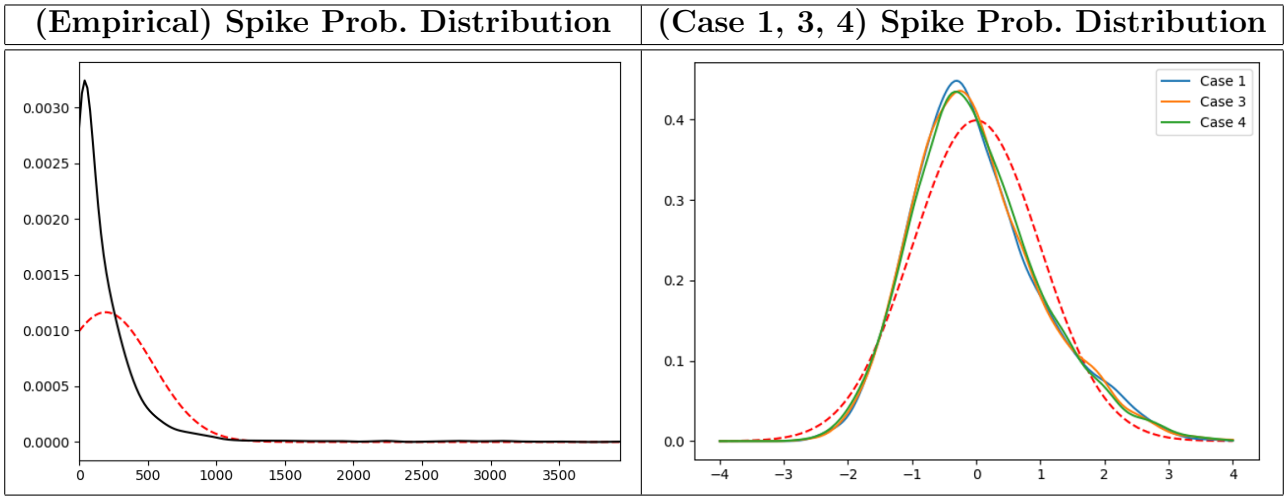

Figure 10: The empirical and model spike probability distribution. There is no significant difference between the distribution curves generated by the models using Case 1, 3 and 4 parameters.

	Min.	Max.	Med.	Mean	Skew.	Ex. Kurt.
Case 1	308	374	330	331.29	0.5945	0.2684
Case 3	297	359	320	320.90	0.5982	0.3511
Case 4	285	345	309	309.88	0.5384	0.3200

Table 9: The quantiles and moments of the spike counts generated by the models using Case 1, 3 and 4 parameters.

There is no significant difference in distribution for Case 1, 3 and 4, and their moments are all of similar orders. No one is strongly preferred over the other, but one way to identify the tail behavior is to consider the *mean-median ratio.* If the ratio is higher, the tail is identified to be longer and more skewed. The ratio is the highest for Case 1. As a multiple of the standard deviation, the maximum spike count of Case 1 is also the furthest away from the mean. *In this sense, Case 1 has the best performance in producing a long tail.* Nonetheless, compared to the empirical distribution, which has a tail that is *significantly* longer, the three cases are still *way* behind.

4.1.2 Spike Counts and Network Features

Case 1, which has parameters $(\epsilon, \alpha) = (0.1, 0.95)$ in the FHN term, is so far the best-performing model – it succeeds in producing neuronal spikes and the spike counts have a long tail. Although the tail is not as as extreme as the empirical one, we are one step closer. A question one may raise is: *Are the spike counts associated in any way with the network features, including degrees and strengths? Further, does the distribution of synaptic strengths affect the distribution of spike counts?* In this part, we attempt to answer the question *in the context of the FHN network model*, so results here are model-specific and do not necessarily generalize to models that obey other kinds of dynamics.

An exploratory data analysis is done to examine how the spike counts depend on the network features. Here, a narrow, but the most plausible, subset of network features is selected, and the spike counts are plotted against each of the network features, which include in-degrees (`k_in`), out-degrees (`k_out`), positive in-degrees (`k_posIn`), in-strengths (`s_in`), out-strengths (`s_out`) and positive out-strengths (`s_posIn`), the definitions of which can be found in the introduction. Some non-linear relations can be seen in all except the `k_out` plot. *It can be concluded that, in general, large spike counts are associated with large degrees and large strengths.* Nodes with moderately large in-degrees and in-strengths can have small spike counts, though.

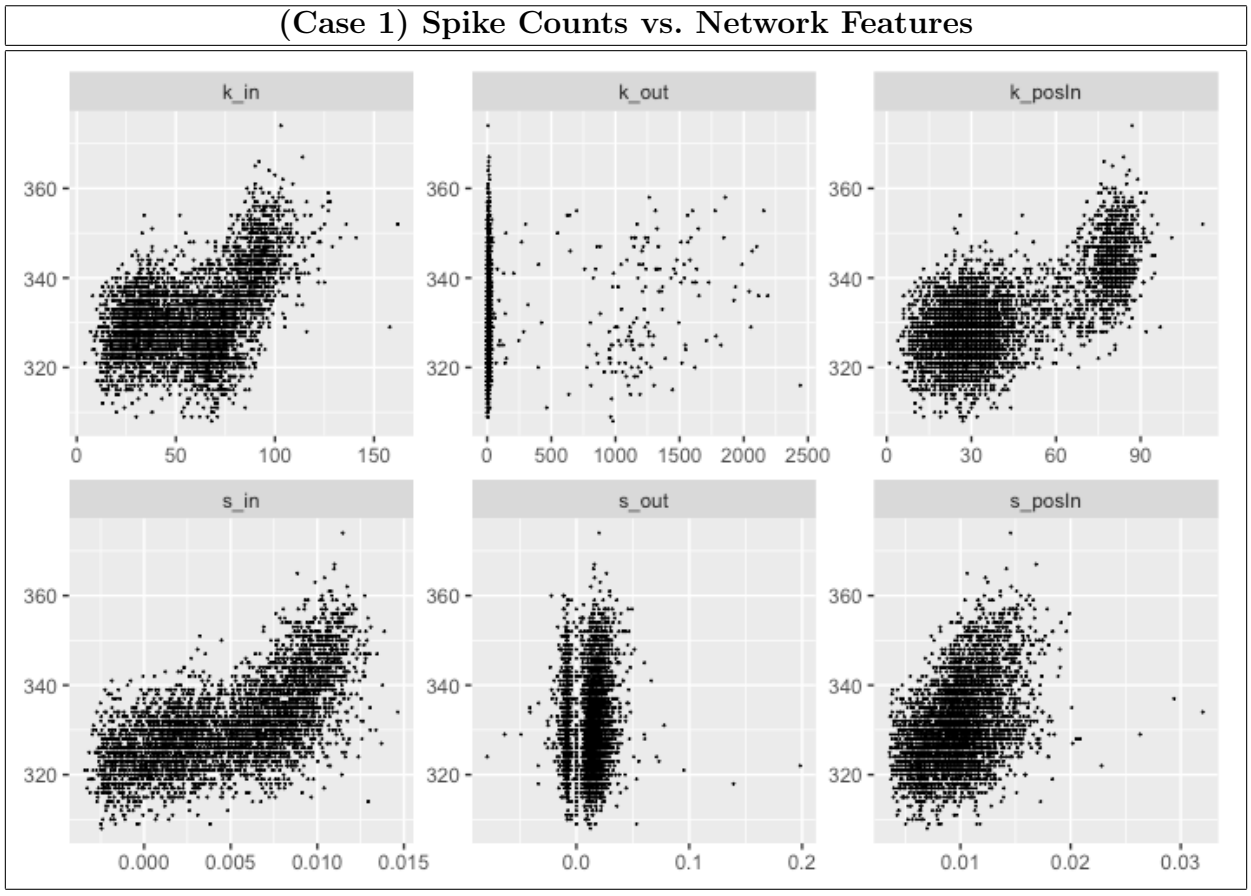

Figure 11: An exploratory analysis on the relations between the spike counts of the Case 1 model and different network features.

To statistically analyze which network features are *truly* important, a linear regression on the features is performed. The feature subset is extended to model non-linearity, and 7 derived features, including `k_in^2`, `k_posIn^2`, `s_in^2`, `s_posIn^2`, `k_in*s_in`, `k_out*s_out` and `k_posIn*s_posIn`, are included additionally as the regressors. To search for the *parsimonious model*, i.e., the model that has the

fewest regressors yet the highest explanatory power (in terms of regression sum of squares), Bayesian information criterion is used. The regression and model selection are respectively done using the `lm` and `stepAIC` function in R. With model simplicity, i.e., number of regressors, taken into account, two are identified as important: `k_in*s_in` and `s_out`. The model statistics are summarized.

$$\text{Spike Count} = 325.4282 + 20.4438 \times \texttt{k\_in*s\_in} - 25.1815 \times \texttt{s\_out} \tag{16}$$

As this is a high-dimensional regression, the signs of the regressors may not be totally trivial. Here, the model tells us that spike counts correlate with `s_out` negatively, which is not immediately obvious from the feature plot above. Meanwhile, spike counts are plotted against `k_in*s_in` and a *strong linearity* is seen. The data points are all contained inside a narrow band around the regression line (in red). Recognize that, for node i, $(\texttt{k\_in*s\_in})_i = \sum_j g_{ij}$ and, therefore, the regression tells us that *spike counts correlate positively with the total incoming coupling strengths*. Physically, why is this the case? At this stage of the project, this is merely an empirical result, which could be an interesting problem for future researchers to work on. While the analysis is not shown here, it is conjectured that *the nodes with high spike counts concentrate in certain regions in the feature space*, and spike counts of an unknown node can potentially be predicted by identifying the cluster in the feature space to which it belongs.

Regressor	**Coefficient**	t**-value**	p**-value**
Intercept	325.4282	2093.95	$< 2 \times 10^{-16}$
`k_in*s_in`	20.4438	72.97	$< 2 \times 10^{-16}$
`s_out`	-25.1815	-3.22	0.00129
Deg. of Freedom	**Res. Std. Error**	R^2	F**-value**
4092	6.137	0.568	2690

Spike Count vs. `k_in*s_in`

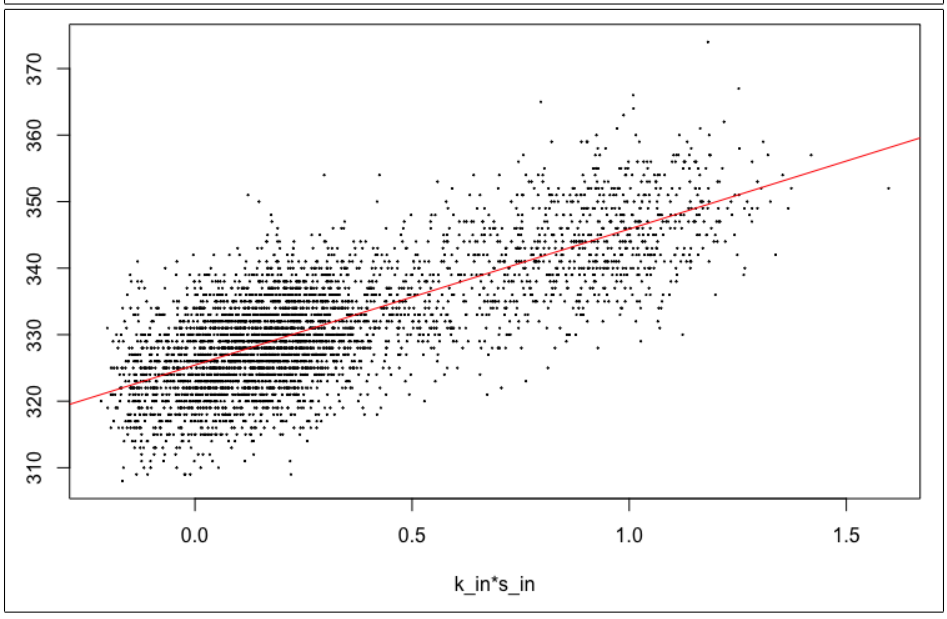

Table 10: The statistics of the regression analysis on the spike counts against features `k_in*s_in` and `s_out` in the parsimonious model. The high F-value suggests a strong linearity in the data and the low p-values suggest that the coefficients are statistically significant. The scatter plot shows the linear correlation between the spike counts and `k_in*s_in`, together with the fitted regression line (red line).

4.1.3 Effects of the Distribution of Synaptic Strength

Regression analysis pinpoints the network features that are *associated with* the spike counts. Going further, another question one may raise is: *What network features cause the spike counts to obey the distribution that they do?* Here, we investigate the causality relation between the network features and the spike counts. We rely on the use of *reference networks*, which are networks derived out of the original network of interest but have certain network features varied and the rest fixed. *Ideally*, *one* particular feature is varied and its effect on the network dynamics can be understood. This, however, is practically impossible given that the network features have strong dependence on each other – they are all derived out of the coupling strength matrix $\mathbf{G}$. When we manipulate a certain feature, some other features are inevitably affected, so no feature can be *marginally* manipulated. In this part, we rely on *a shuffling technique* to derive reference networks out of the original network with the reconstructed $\mathbf{G}$, in an attempt to maximally preserve the other features while manipulating certain features of interest. This was inspired by the bootstrap technique in non-parametric statistics, which allows the generation of new samples that approximately obey the distribution that the original dataset respects through sampling with replacement, with the modification that, instead of sampling, *shuffling* is used.

The following reference networks are designed. Based on the original network with reconstructed coupling strengths g_{ij},

- (*Reference Network 1*) The non-zero g_{ij} are replaced with samples from $\mathcal{N}(\mu, \sigma)$, where μ and σ are respectively the mean and the standard deviation of the non-zero g_{ij}.
- (*Reference Network 2*) For each i, g_{ij} are shuffled. Effectively, each row in $\mathbf{G}$ is replaced by a permuted vector of all entries (zeros included) in the row.
- (*Reference Network 3*) For each j, g_{ij} are shuffled. Effectively, each column in $\mathbf{G}$ is replaced by a permuted vector of all entries (zeros included) in the column.
- (*Reference Network 4*) An independently generated DWR network using the same connection probability $p = \sum \mathbb{1}(g_{ij} \neq 0)/N(N-1)$ with coupling strengths sampled from $\mathcal{N}(\mu, \sigma)$.
- (*Reference Network 5*) The non-zero g_{ij} are shuffled.

The computational construction and the intention of each reference network are summarized.

Ref. Net.	Computational Construction	Intention
1	Non-zero $g_{ij} \to \mathcal{N}(\mu, \sigma)$	Keep $\{k_{\text{in}}(i), k_{\text{out}}(i)\}$ but vary $\{s_{\text{in}}(i), s_{\text{out}}(i)\}$
2	Shuffle rows in $\mathbf{G}$	Keep $\{k_{\text{in}}(i), s_{\text{in}}(i)\}$ but vary $\{k_{\text{out}}(i), s_{\text{out}}(i)\}$
3	Shuffle columns in $\mathbf{G}$	Keep $\{k_{\text{out}}(i), s_{\text{out}}(i)\}$ but vary $\{k_{\text{in}}(i), s_{\text{in}}(i)\}$
4	DWR network	All network features are structure-free
5	Shuffle non-zero entries in $\mathbf{G}$	Keep $\{k_{\text{in}}(i), k_{\text{out}}(i)\}$ but vary $\{s_{\text{in}}(i), s_{\text{out}}(i)\}$

Table 11: The computational construction and the intention of the five reference networks used for understanding the effects of the varied network features.

There is an interesting (though irrelevant) remark on ref. net. 1 and 5. While, for their different constructions, the coupling strengths of ref. net. 1 obey a Gaussian and that of ref. net. 5 obey the original long-tailed distribution discussed, the standardized distributions of their $s_{\text{in/out}}(i)$ are actually very similar in shape. Both are seen to deviate from the standard Gaussian (red dashed line) and have taller peaks. For ref. net. 1, the distribution can be understood as follows. Consider $s_{\text{in}}(i)$, which, computationally, is the average of the non-zero entries of row i in $\mathbf{G}$. By construction, non-zero $g_{ij} \sim \mathcal{N}(\mu, \sigma)$ and, as $s_{\text{in}}(i)$ is the average of $k_{\text{in}}(i)$ such Gaussian random numbers, $s_{\text{in}}(i) \sim \mathcal{N}(\mu, \sigma/\sqrt{k_{\text{in}}(i)})$. But for different i, $s_{\text{in}}(i)$ obeys a different Gaussian and, collectively,

the distribution of all $s_{\text{in}}(i)$ is thus deviating from Gaussian, and is formally known as a mixture distribution of Gaussians. It is not expressible in a closed-form formula. Similar argument also applies to $s_{\text{out}}(i)$. For ref. net. 5, suppose that the non-zero g_{ij} are identically and independently sampled from a certain (unknown) distribution that has mean μ and s.d. σ. For a sufficiently large $k_{\text{in}}(i)$, by the central limit theorem, still $s_{\text{in}}(i) \sim \mathcal{N}(\mu, \sigma/\sqrt{k_{\text{in}}(i)})$, at least approximately. $k_{\text{in}}(i)$ is not small for a majority of the nodes, so the approximation is expected to work moderately well. *Therefore, we can see that for ref. net. 1 and 5, even through their underlying g_{ij} obey two totally different distributions, their $s_{\text{in/out}}(i)$ can still turn out to be distributed similarly.*

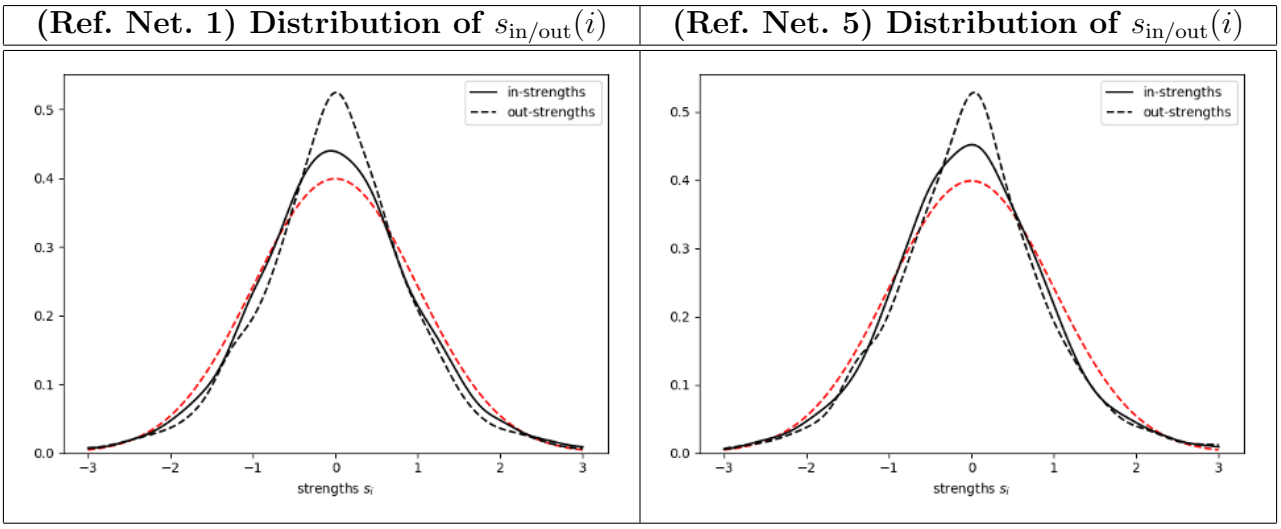

Figure 12: The probability distribution of $s_{\text{in/out}}(i)$ of reference network 1 and 5, which are similar despite their differently constructed **G**.

For the reference networks, *the effects of the varied network features* are what we seek to investigate. For each, the FHN network model combined with the diffusive nodal interaction, *assuming the constructed reference coupling strength matrix* **G**, is run and the model time series are returned. If, for example, using ref. net. 2, the spiking dynamics turns out to be similar to what the original network produces, then we can conclude that network features $k_{\text{out}}(i)$ and $s_{\text{out}}(i)$ are not important driving factors for the spiking dynamics while $k_{\text{in}}(i)$ and $s_{\text{in}}(i)$ *probably* are. (As we shall see, this is indeed the case.) Note again that the features being *kept* have distributions *identical* to that of the original network, which are long-tailed and contain its "unique structure", while the features being *varied* have distributions *close to Gaussian*. Interested readers may refer to the appendix for the precise distributions of the in/out-strengths for the reference networks.

The probability distributions of the standardized spike counts of the five ref. net. are shown. The distributions of ref. net. 1, 3, 4 and 5, despite some amount of deviation at the middle, are well approximated by the standard Gaussian (red dashed line), which has a large degree of overlapping with the distribution of ref. net. 4. In contrast, the distributions of the original network and ref. net. 2 are similar in shape, and are both deviating from the Gaussian with a long right tail. Recall that ref. net. 2 has the rows in the original reconstructed coupling strength matrix **G** shuffled and, therefore, $\{k_{\text{in}}(i), s_{\text{in}}(i)\}$ are preserved but $\{k_{\text{out}}(i), s_{\text{out}}(i)\}$ are varied. That it has a spike probability distribution close to the original implies that $k_{\text{out}}(i)$ and $s_{\text{out}}(i)$ are not important driving factors of the spiking dynamics while $k_{\text{in}}(i)$ and $s_{\text{in}}(i)$ *could be*. For ref. net. 1 and 5, $\{k_{\text{in}}(i), k_{\text{out}}(i)\}$ are preserved but $\{s_{\text{in}}(i), s_{\text{out}}(i)\}$ are varied. The preservation of $k_{\text{in}}(i)$ does not leave the spike probability distribution unchanged; instead, it becomes a Gaussian. Thus, we can further rule out $k_{\text{in}}(i)$ as a driving factor of the spiking dynamics. *In summary, through understanding the effects of the varied*

network features of the ref. net., only $s_{\text{in}}(i)$ is identified to be the factor that affects the spiking dynamics.

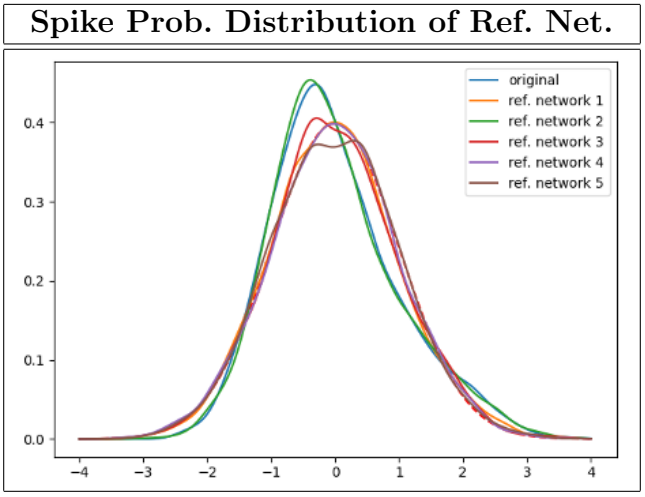

Figure 13: The probability distribution of the standardized spike counts of the five reference networks. That of ref. net. 2 is similar to the original while the rest are close to the standard Gaussian (red dashed line).

The correlations between the spike counts and the network features for the ref. net. are also looked at to reinforce the above argument. Here, only plots of ref. net. 2 and 4 are examined and for the rest, interested readers may refer to the appendix. For ref. net. 2, by construction, the `k_in`, `k_posIn`, `s_in` and `s_posIn` plots are almost identical to that of the original network. In other words, even though the distributions of $k_{\text{out}}(i)$ and $s_{\text{out}}(i)$ are disrupted by the row-shuffling during the construction of ref. net. 2, the correlation structures between the spike counts and the different in-measures, including `k_in` and `s_in`, are well preserved. *This again confirms that the distributions of the out-measures do not have an important effect on the spiking dynamics while the distributions of the in-measures do.* We have seen that *both* the incoming strengths and the spike counts have a long-tailed distribution – this is also what motivates this research project. *Are they associated?* The plots suggest an affirmative answer, at least in the context of this FHN network model with the diffusive nodal interaction. In the `s_in` plot, large `s_in` is associated with large spike counts – they respectively correspond to the tail in the incoming strength distribution and the spike distribution.

For ref. net. 4, as it is an independently generated DWR network with Gaussian coupling strengths, the network measures, including degrees and strengths, all *approximately* obey a Gaussian distribution, lacking any "special structure". As we have excluded `k_out` and `s_out` as the driving factors of the spiking dynamics, their plots are not useful to look at. Rather, for the in-measures, they all obey an uninteresting Gaussian distribution and, as a result, the spike counts are Gaussian. This explains why the data points are distributed in an elliptical region.

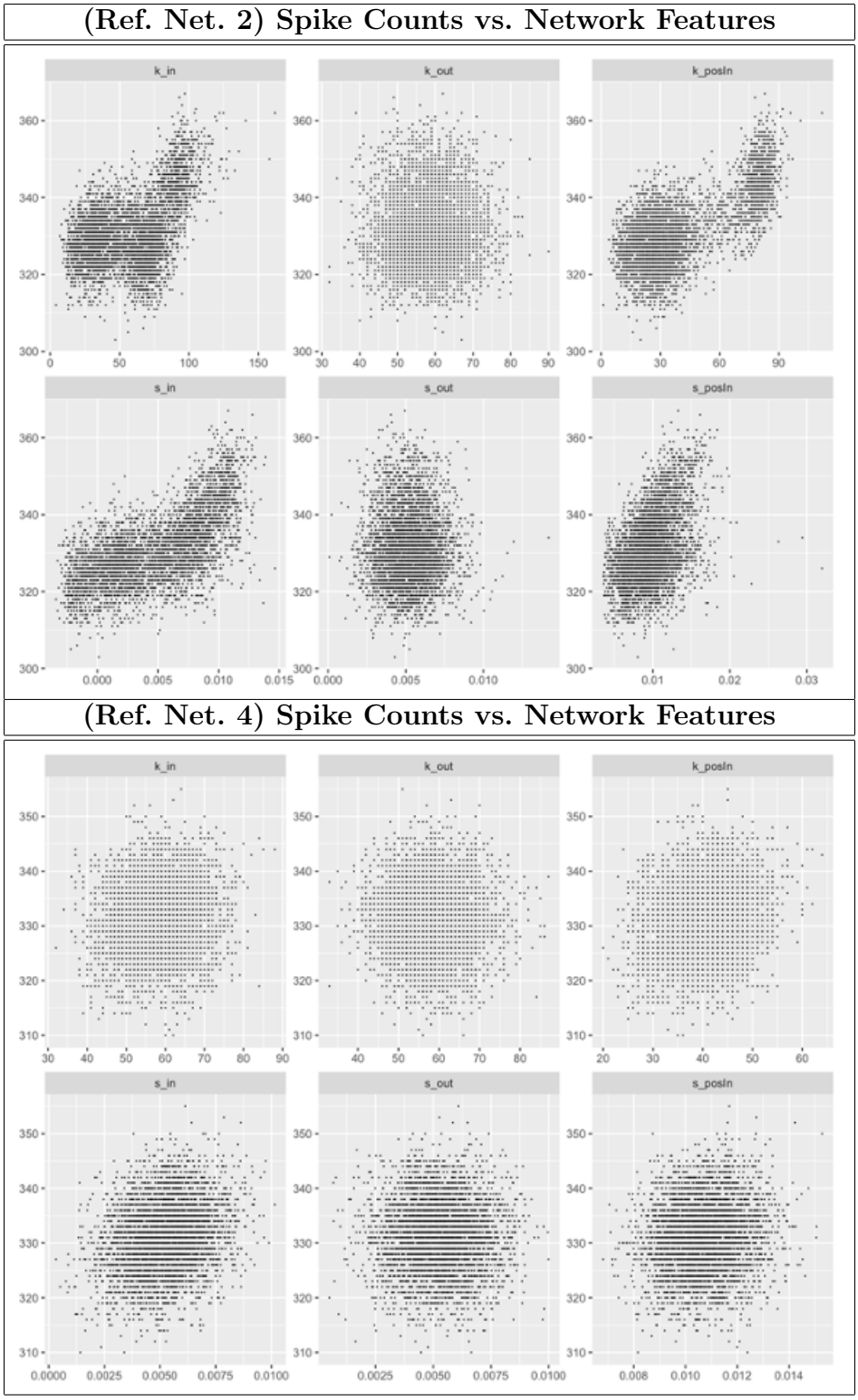

Figure 14: The relations between the spike counts of ref. net. 2 and 4 and different network features.

4.2 Synaptic Nodal Interaction

The *FHN* network models combined with the *synaptic* nodal interaction h^{syn} and using the following tabulated set of parameters are investigated.

Type	**Settings and Parameters**
Network	Based on the reconstructed coupling strength matrix $\mathbf{G}$ ($N = 4095$)
Dynamics	$(Intrinsic)$ $f_i^x(x,y) = (x - x^3/3 - y)/\epsilon$, $f_i^y(x,y) = x + \alpha$ $(Interaction)$ $h^{\text{syn}}(x,y) = 1/\beta_1\{1 + \tanh[\beta_2(y - y_0)]\}$, $(\beta_1, \beta_2, y_0) = (0.01, 1, 0)$ $(Noise)$ $D_{ij} = \sigma_i^2 \delta_{ij}, \sigma_i = 2$
Initial Conditions	$x_i(t = 0) \sim \mathcal{U}[-1, 1]$
Computational Settings	Step size $\delta t = 5 \times 10^{-4}$, time steps $N_{\text{data}} = 2 \times 10^6$

Table 12: Settings and parameters of the FHN network model with the synaptic nodal interaction.

Spiking dynamics are successfully generated by the model. Signs of a long-tailed spike distribution are seen. For example, comparing the time series of node 0 and 40 over the time interval $[500, 520]$, the spiking activity of node 0 is significantly more active, though the spikes experience a shorter time scale.

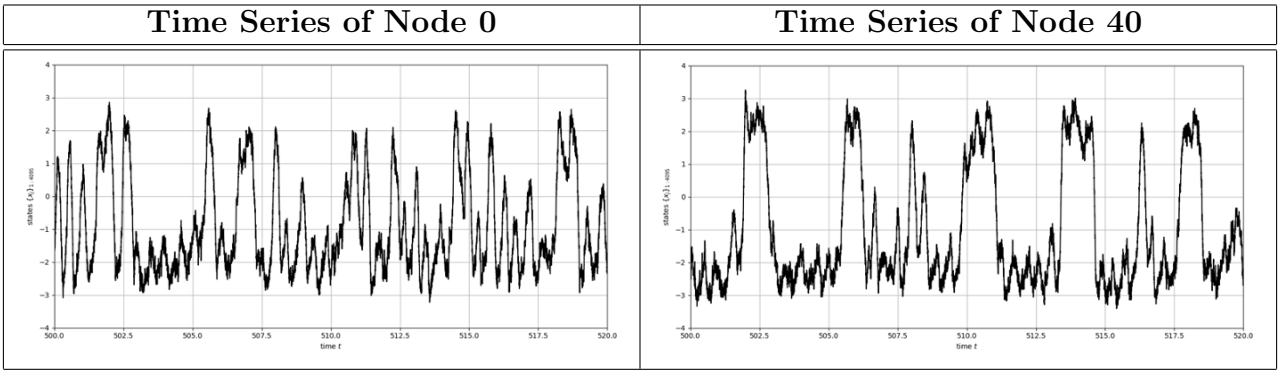

Figure 15: Time series of node 0 and 40 over the time interval $[500, 520]$. Node 0 has a more active spiking dynamics than node 40, with the spikes in a shorter time scale.

Using the same peak detection algorithm with the same conditions that spikes (1) lie above $h = 0$ and (2) are at least separated by $d = 2000$ time steps, the detected spikes lead to the following spike probability distribution. A Gaussian (red dashed line) with the same mean and s.d. is shown to contrast. On the other hand, the spike probability distributions (1) observed experimentally, (2) generated by the FHN network model with the diffusive nodal interaction and (3) with the synaptic nodal interaction are compared. The blue curve corresponds to the empirical spike distribution discussed in the introduction, while the orange curve corresponds to that in the previous section using the Case 1 parameters, but standardized. We can see an improvement of the synaptic model over the diffusive model. It has a large concentration of nodes with spike counts near the mean, with some portion of nodes having spike counts extending far beyond the mean. The maximum spike count is at 5 standard deviations. This is closer to the behavior of neuronal spikes experimentally observed. The improvement is clear from the comparison plot, where, for the experimental and synaptic model curve, we can see an exponential-like decay.

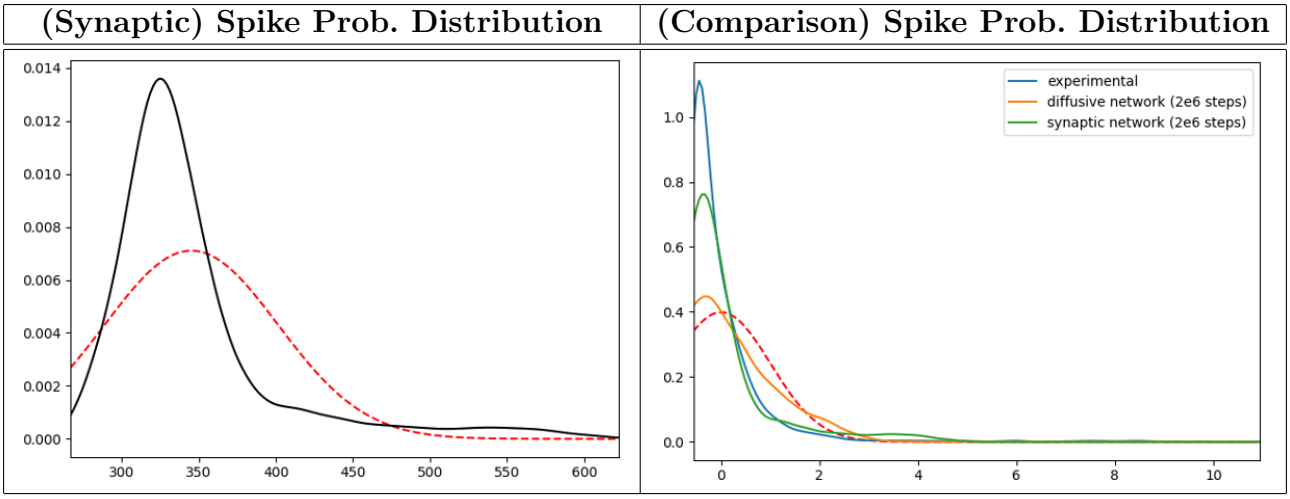

Figure 16: The spike probability distribution of the synaptic model and a comparison of the performance of the diffusive and synaptic model (both assuming the FHN intrinsic dynamics). The synaptic model is seen to produce a spike probability distribution close to the empirical result.

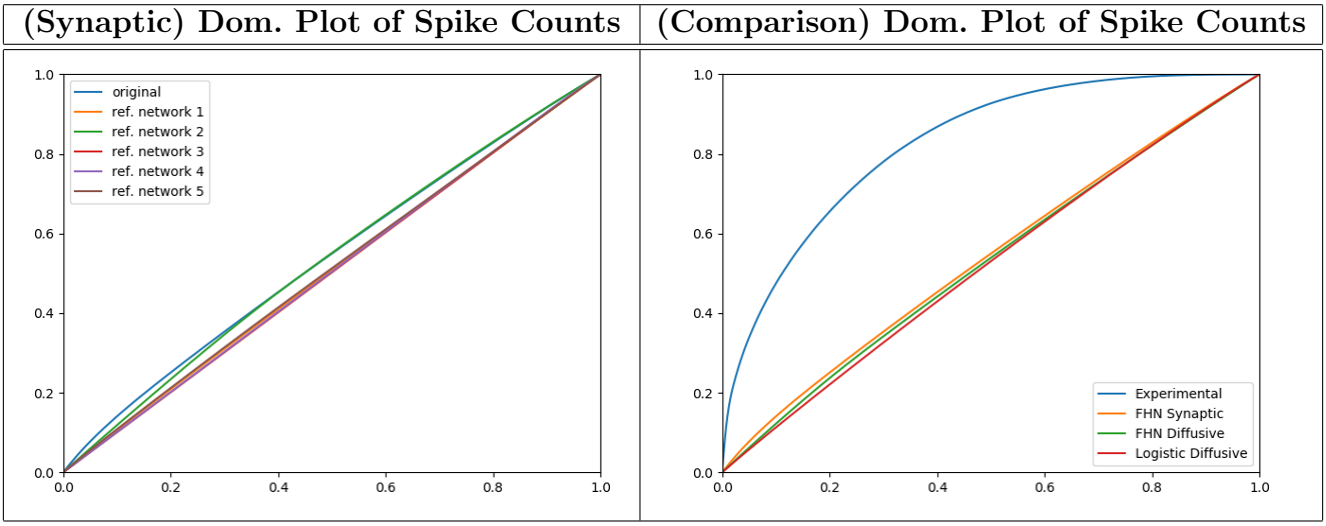

Figure 17: The dominance plot of the spike counts generated by the original network and the five reference networks assuming the synaptic nodal interaction. Ref. net. 2 produces a curve close to the original network. The other plot shows a comparison of the different models tested in this project. The FHN network model with the synaptic nodal interaction is considered the most successful as it has the highest curvature and is able to produce realistic spikes, which, however, is still not as extreme as the experimental result. Still, this is a significant improvement compared to what we have started – the logistic model shows completely no sign of spikes.

For the diffusive nodal interaction, we have concluded that $s_{\text{in}}(i)$ is the driving factor for the spiking dynamics. The result is model-specific and do not necessarily generalize when we assume other kinds of dynamical functions. For the synaptic nodal interaction, we may ask the same question – *is* $s_{\text{in}}(i)$ *still a driving factor for the spiking dynamics?* The following analysis answers in the affirmative. The exact same set of reference networks is used, and their spiking dynamics are investigated. *It is seen from the dominance plot that, still, ref. net. 2 is able to mimic the dynamics of the original synaptic network to the greatest extent.* A *dominance plot* illustrates the fraction of the total explained by the largest n data, and can be constructed by (1) ordering the data from the largest to the smallest and (2) connecting data points $(n/N, \sum_{i=1}^{n} X_i/S)$ for $n = 1, 2, ..., N$, with N being the number of data and S being the sum of all data. The dominance plot is commonly used for analyzing the behavior of the data lying in the tail. The more curvature the plot shows, *the longer the tail is and*

the further away from the mean the extreme outliers are. Here, we use the dominance plot to contrast the curvatures that different reference networks give. The dominance curves of the spike counts of the original network, based on the reconstructed $\mathbf{G}$, and ref. net. 2, based on the row-shuffled $\mathbf{G}$, have similar curvature. The other ref. net., on the other hand, lack any obvious curvature, which implies that the large spike counts generated by the models are actually "not too far away" from the mean. Ref. net. 2 preserves $s_{\text{in}}(i)$ and the dominance curve of spike counts is still comparable to the original, *therefore it is concluded that, for the synaptic nodal interaction,* $s_{\text{in}}(i)$ *is still the driving factor for the spiking dynamics.*

To summarize the different models tested in this project, as seen from the dominance plot comparison on right panel, *the FHN network model with the synaptic nodal interaction is the most successful in replicating the neuronal spikes*, which empirically are highly skewed and have a long tail in distribution. In the spike probability distribution plot, the tail of the synaptic model resembles the experimental one, both showing an exponential-like decay. The dominance plot offers a new perspective to understand the behavior of the extreme outliers, and we can see from the comparison plot that, assuming the FHN intrinsic dynamics, *the synaptic model is better at producing a curvature than the diffusive model. The logistic network model with the diffusive nodal interaction has the worst performance*, with a curve that is almost entirely flat. We have seen from the prior analysis that the model even fails at generating realistic neuronal spikes, so it is an inferior model. Nonetheless, despite the improvements in replicating the spiking dynamics, the three models are still far from achieving the extreme curvature that the empirical neuronal spikes exhibit, so there is still a long way to go. Despite this, the improvements in the models have been significant – *from the initial logistic model showing completely no sign of spikes to the FHN model showing a long-tailed spiking dynamics when combined with the synaptic nodal interaction.*

5 Conclusion

There are many measures to aid us in understanding a network. In this project, we focus on degrees, including the in-degrees $k_{\text{in}}(i)$ and the out-degrees $k_{\text{out}}(i)$, and strengths, including the in-strengths $s_{\text{in}}(i)$ and the out-strengths $s_{\text{out}}(i)$. The network reconstruction method reviewed, which is proposed by Ching and Tam, is used to extract the coupling strengths g_{ij} based on neuronal time series data experimentally collected, and with the reconstructed coupling strength matrix $\mathbf{G}$, different combinations of intrinsic dynamics and nodal interaction are attempted. For the *logistic network model*, which is a one-dimensional model with the logistic intrinsic dynamics, the time series generated fail to produce realistic spiking dynamics, and only fluctuations, rather than spikes, are observed. The *FHN network model*, which is a two-dimensional model with the FHN intrisic dynamics, shows a great improvement. The time series generated are realistic with active spiking activity. The synaptic model is superior to the diffusive model as it is able to produce a spike distribution curve with a higher skewness and a longer tail. To understand the relation between the long-tailed spike counts and different network features, two methods are used – *regression analysis* and *comparison with reference networks*, which have artificially constructed $\mathbf{G}$ to vary some features of interest while preserving the other. From the feature plots, we see some non-linear relations between the spike counts and different network in-measures, while relations with the out-measures are ambiguous, and we can conclude that *the spiking dynamics depends more importantly on the in-measures*. With the reference networks, the long-tailed *incoming strengths* $s_{\text{in}}(i)$ are determined to be the driving factor for the long-tailed spike counts. The distribution of $s_{\text{in}}(i)$ is found to have a concrete effect on the distribution of spike counts, as ref. net. 2, which preserves $s_{\text{in}}(i)$, generates heavy-tailed spike counts while the other ref. net. have $s_{\text{in}}(i)$ that are approximately Gaussian and so do their generated spike counts. Through comparing the ref. net., we can also rule out other network features as driving factors. Therefore, to answer the questions in the objectives,

(1) For the FHN network model, the long-tailed distribution of *incoming strengths* $s_{\text{in}}(i)$ leads to the long-tailed spike counts while other network features have no obvious effect on the spiking dynamics.

(2) The *FHN network model with the synaptic nodal interaction* has the best performance in reproducing spike counts and is able to recover some of the empirical statistical features, such as the high skewness and the long tail. However, the dominance curve is still far from achieving the curvature that the experimental spike counts have, so there is still a lot of room for improvement, and the search for realistic models of neurons will still continue.

6 Datasets and Codes

All datasets and codes necessary for replicating the simulation results in this project are here. The data format and their usage are discussed below.

There are two dataset files, namely `DIV25_PREmethod` and `DIV25_spks`.

- (*Reconstructed* $\mathbf{G}$) `DIV25_PREmethod` contains the reconstructed coupling strengths g_{ij} in the format described in the introduction, and is provided by my supervisor. Each row takes the format `i j g_ij`, and `g_ij` is the coupling strength of the edge linking from node `j` to node `i`. Unstated node pairs are implied to be unconnected. The file is all the data necessary to construct a network.
- (*Spike Counts*) `DIV25_spks` contains the spike count data of collected by the 4095 electrodes, which measure the electrical signals generated by the rat embryonic neurons over 25 dats in vitro. Each row takes the format `n t1 t2 ... tn`, where `n` is the total spike counts of a specific node measured over the period and `t1, t2, ..., tn` are the computational time steps at which a spike is detected to occur. In this project, only the first datum in the rows is used and the subsequent data, representing the spike timing, are not analyzed, which, however, constitute another important characterization of a neuronal dynamics. Looking at the first few rows of the data file immediately tells us that heavy-tailed nature of neuronal spikes – the first node has 521 spikes while the subsequent few have less than 10, which is a very sharp contrast.

For the codes, only an overview is provided here and the computational details are not discussed. The codes consist of two parts, namely the `graph` class and the `network` class. The following distinction is made: `graph` represents the underlying network structure and all variables contained inside the class are derived from the coupling strength matrix $\mathbf{G}$ read in or internally constructed, while `network`, inheriting from the `graph` class, represents the dynamics generated by the network model after desired dynamical functional forms, for both the intrinsic dynamics and the nodal interaction, are selected. The most important variables and functions for the two classes are listed below. Functions are followed by a bracket `()` and the arguments, if any, are omitted.

- `graph` class:
  - `size`: the number of nodes in the graph
  - `Coupling`: the coupling strength matrix
  - `Adjacency`: the adjacency matrix derived from `Coupling`, with entries $A_{ij} = \mathbb{1}(g_{ij} \neq 0)$
  - `initialize()`: compute all the network measures that may be of interest, for example, in-degrees (`degrees_in`) and in-strengths (`strengths_in`)
- `network` class:
  - `intrinsicFunc()`: the logistic intrinsic dynamics functions
  - `intrinsicFunc_FHN()`: the FHN intrinsic dynamics functions
  - `couplingFunc_diffusive()`: the diffusive nodal interaction functions
  - `couplingFunc_synaptic()`: the synaptic nodal interaction functions
  - `initDynamics()`: initialize a one-dimensional logistic dynamics by passing in the initial conditions, coefficients for the intrinsic dynamics and covariance of noise
  - `initDynamics_FHN()`: same as above but assuming a two-dimensional FHN dynamics
  - `getStateChanges()`: compute the changes in the nodal states over a computational time step
  - `runDynamics()`: iteratively update the nodal states using the Euler-Maruyama algorithm until the final time step is reached

The other functions in the `network` class are for analysis purpose and are mainly used to generate

plots. Some examples include `findpeaks()`, which locates the spikes using the peak selection numerical criterion discussed, `plotDynamics()`, which plots the time series of the nodal states, and `plotPeakCountDist`, which plots the probability distribution curve of the spike counts. Functions labeled with `# DEPRECATED` are ad hoc or used for temporary testing, and are foreseen to be used rarely in any future analysis.

7 Acknowledgments

The author thanks Prof. Ching for her advice and guidance throughout the research project and on this report.

8 References

[1] S. H. Strogatz, Exploring complex networks, Nature (London) 410, 268 (2001).

[2] B. Albert-László and A. Réka, Emergence of scaling in random networks, Science. 286 (5439): 509–512.

[3] J. M. Stuart, E. Segal, D. Koller and S. K. Jim, A gene-coexpression network for global discovery of conserved genetic modules, Science 302, 249 (2003).

[4] D. Yu, M. Righero and L. Kocarev, Estimating Topology of Networks, Phys. Rev. Lett. 97, 188701 (2006).

[5] E. S. C. Ching and H. C. Tam, Reconstructing links in directed networks from noisy dynamics, Phys. Rev. E 95, 010301(R) (2017).

[6] C. Sun, K. C. Lin, Y. T. Huang, E. S. C. Ching, P. Y. Lai and C. K. Chan, Directed effective connectivity and synaptic weights of in vitro neuronal cultures revealed from high-density multielectrode array recordings, BioRxiv 2020.02.06.936781 [Preprint], available from https://doi.org/10.1101/2020.02.06.936781.

[7] G. Buzsáki and K. Mizuseki, The log-dynamic brain: how skewed distributions affect network operations, Nat. Rev. Neurosci., 2014;15(4):264-278.

[8] L. Kuśmierz, S. Ogawa, and T. Toyoizumi, Edge of Chaos and Avalanches in Neural Networks with Heavy-Tailed Synaptic Weight Distribution, Phys. Rev. Lett. 125, 028101 (2020).

9 Appendix

Here, the feature plots of the original network and the five reference networks are shown. The original network obeys the reconstructed coupling strength matrix **G** while the reference networks obey their respective constructed **G**. They all respect the *FHN* intrinsic dynamics and the *diffusive* nodal interaction. Compared to the original network, for ref. net. 2, the relations between the spike counts and different in-measures are basically preserved, while for the other ref. net., the spike counts no longer have a long-tailed distribution as the "structures" in the in-measures, in particular the incoming strength `s_in`, are disrupted through the shuffling construction.

(Original) Spike Counts vs. Network Features

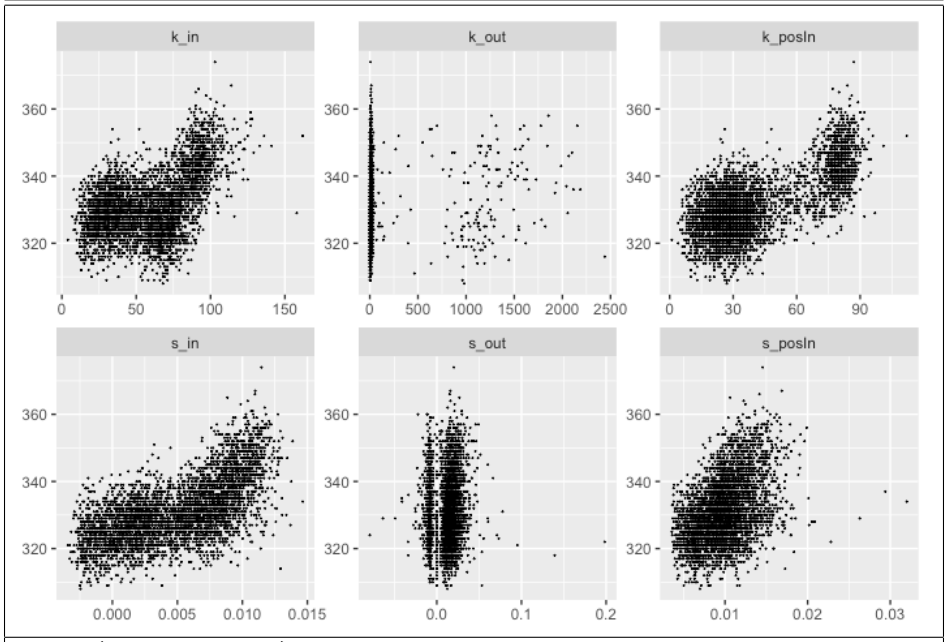

(Ref. Net. 1) Spike Counts vs. Network Features

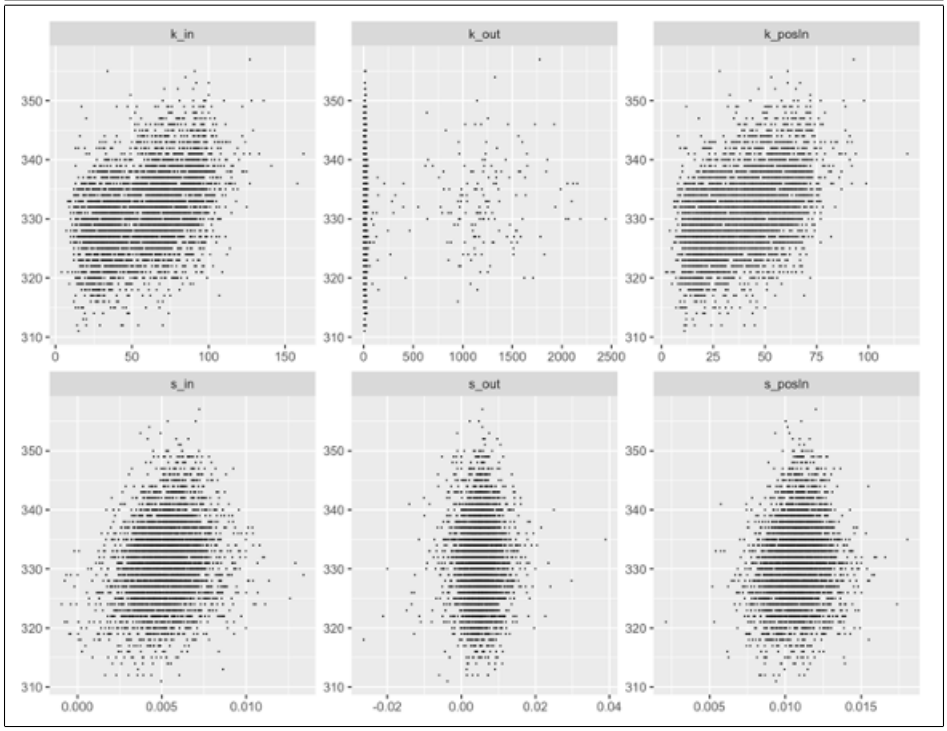

(Ref. Net. 2) Spike Counts vs. Network Features

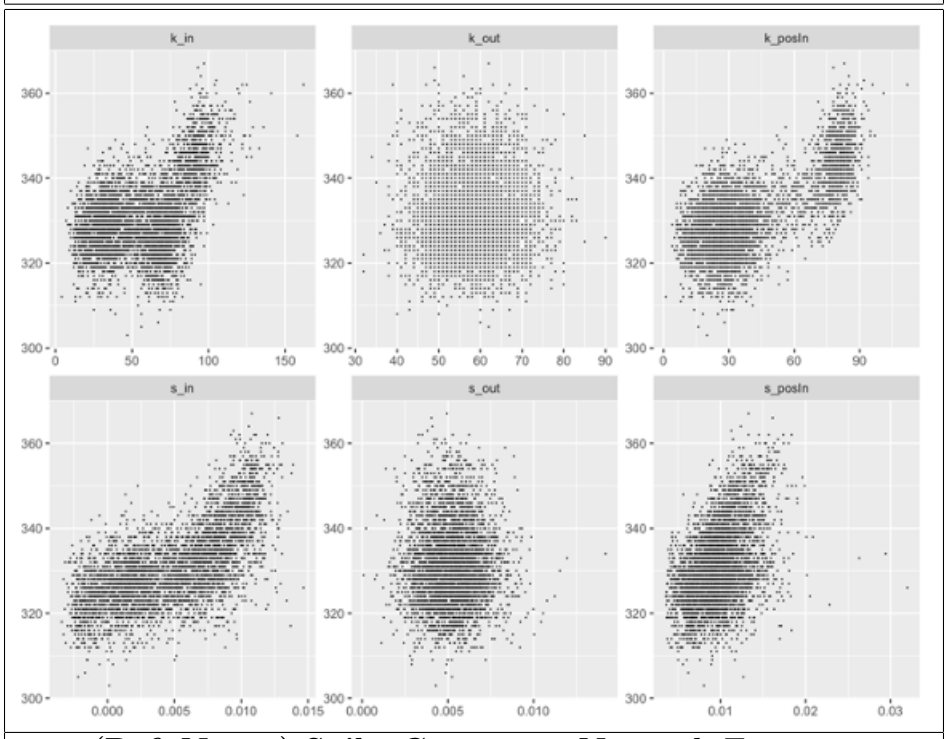

(Ref. Net. 3) Spike Counts vs. Network Features

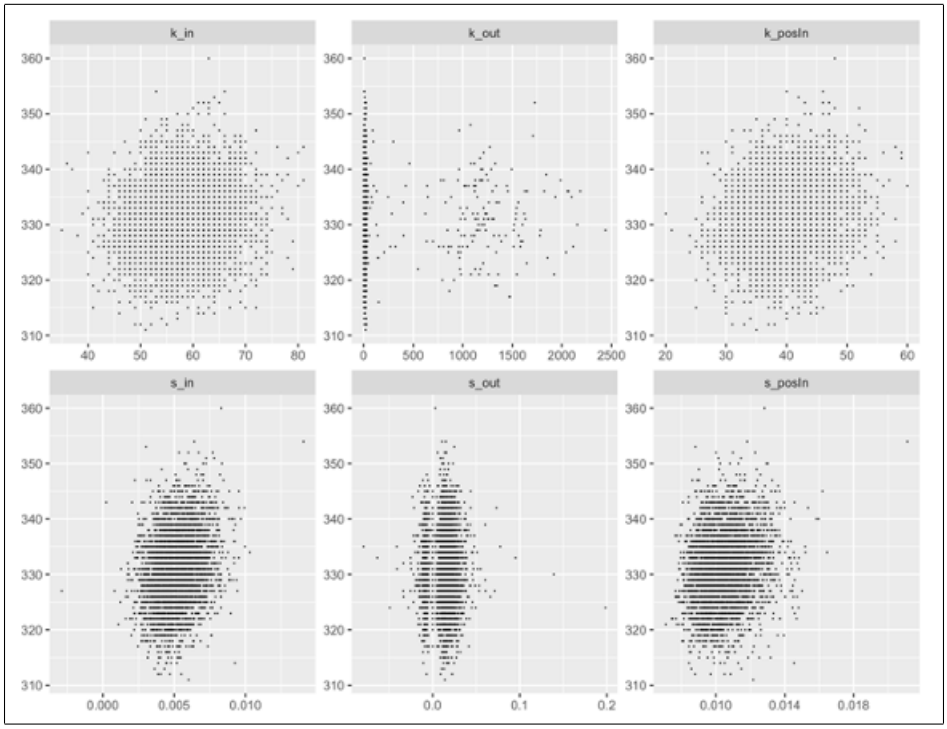

(Ref. Net. 4) Spike Counts vs. Network Features

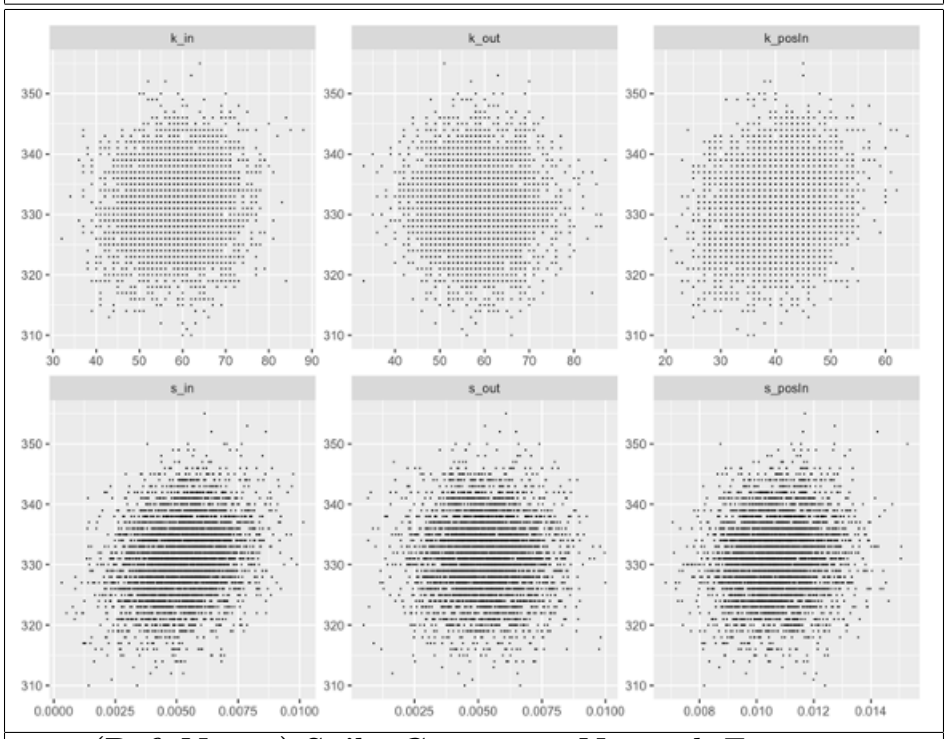

(Ref. Net. 5) Spike Counts vs. Network Features

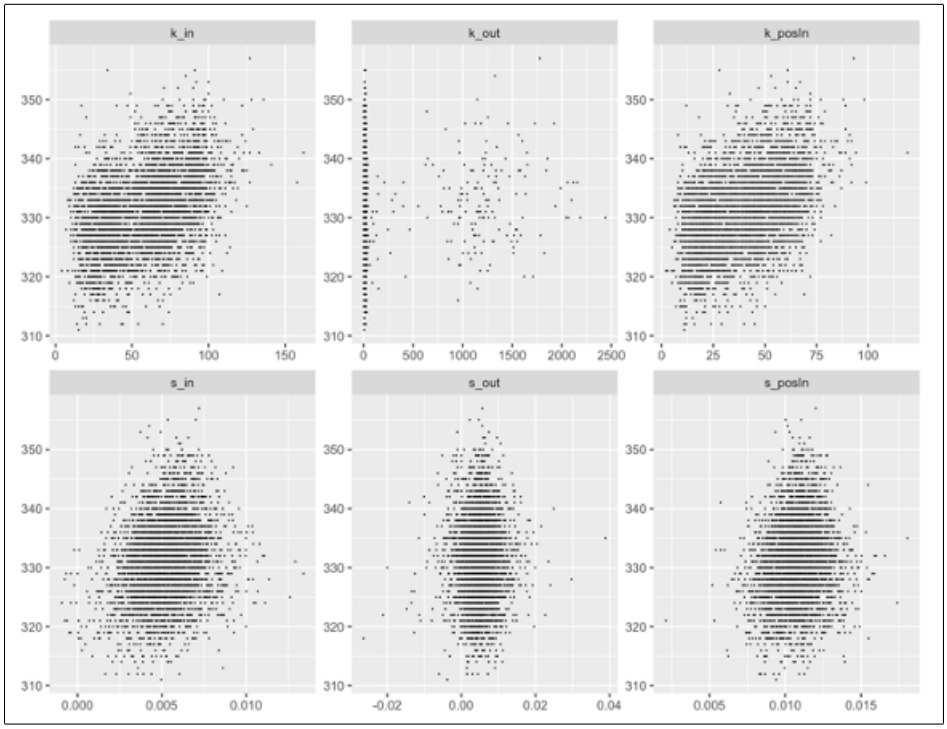

Here, the distributions of the standardized strengths for the reference networks are shown. The ref. net. have certain features left untouched while some other varied. The network features being kept have distributions identical to that of the original network, while those being varied have bell-shaped distributions close to Gaussian. As an example, the coupling strength matrix $\mathbf{G}$ of ref. net. 2 has the rows shuffled, keeping $\{k_{\rm in}(i), s_{\rm in}(i)\}$ while varying $\{k_{\rm out}(i), s_{\rm out}(i)\}$. Therefore, we can see that the distribution of the in-strengths is preserved (identical to the original) but the distribution of the out-strengths becomes close to Gaussian (the long-tailed structure is destroyed through shuffling). The effects of the varied network features are studied.

(Original) Distribution of $s_{\rm in/out}(i)$

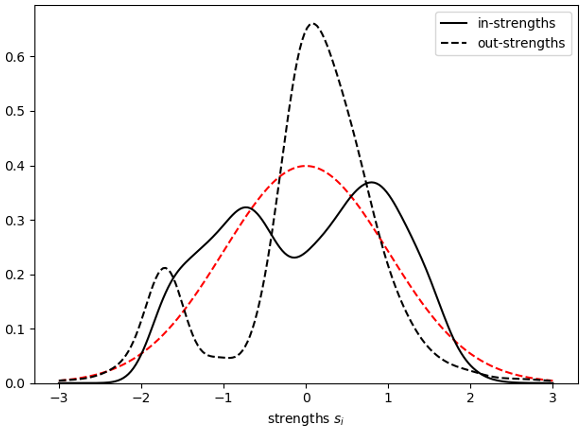

(Ref. Net. 1) Distribution of $s_{\rm in/out}(i)$

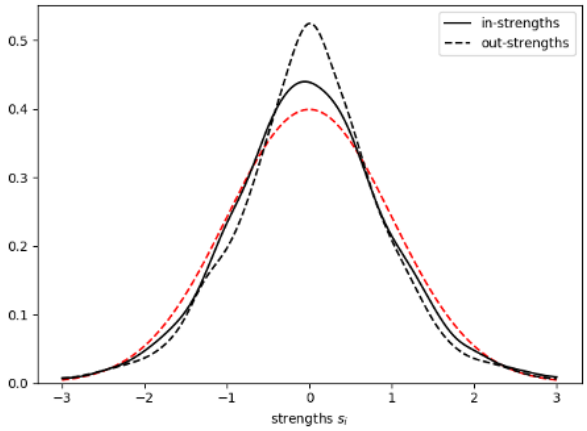

(Ref. Net. 2) Distribution of $s_{\rm in/out}(i)$

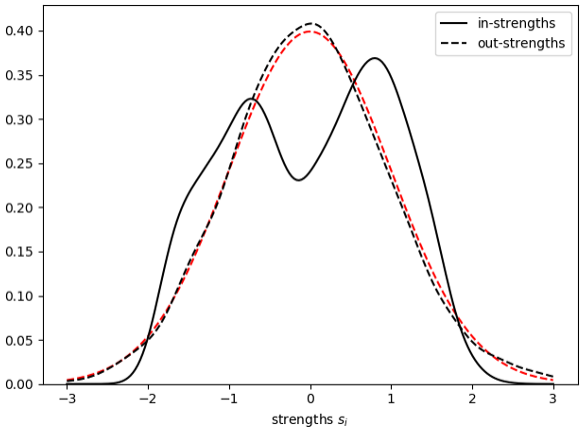

(Ref. Net. 3) Distribution of $s_{\rm in/out}(i)$

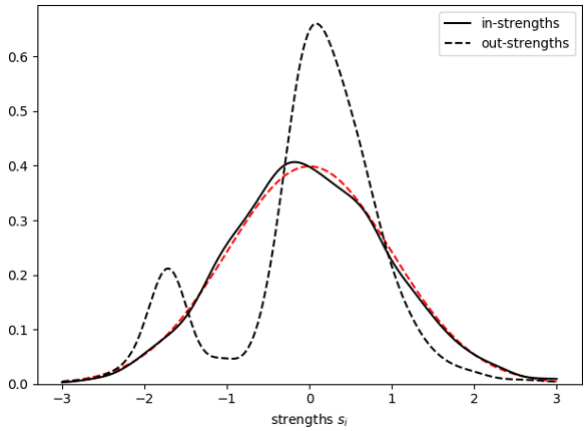

(Ref. Net. 4) Distribution of $s_{\rm in/out}(i)$

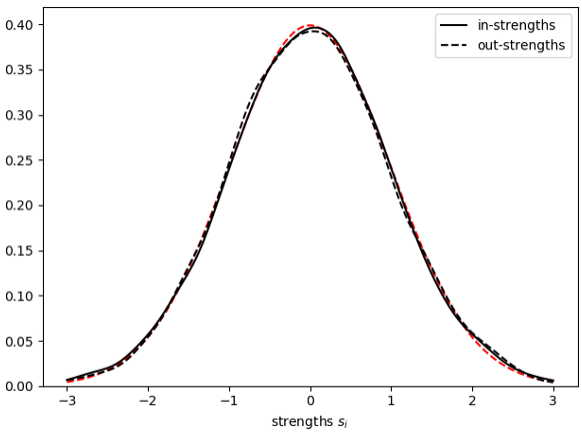

(Ref. Net. 5) Distribution of $s_{\rm in/out}(i)$